~~Comparison~~ Comparison of temperature and wind between ground-based remote sensing observations and NWP model profiles in complex topography: the Meiringen campaign

Alexandre Bugnard1, Martine Collaud Coen1, Maxime Hervo1, Daniel Leuenberger1, Marco Arpagaus1, and Samuel Monhart1

1Federal Office of Meteorology and Climatology, MeteoSwiss, Switzerland
Correspondence: Martine Collaud Coen (martine.collaud@meteoswiss.ch)

Abstract. Thermally driven valley winds and near-surface air temperature inversions are common over complex topography and have a significant impact on the local and mesoscale weather situation. They both affect the dynamics of air masses and pollutant concentration. Valley winds affect ~~it~~ them by favoring horizontal transport and exchange between the boundary layer and the free troposphere, ~~and temperature inversion by concentrating pollutants in cold stable surface layers. The complex interactions that lead to the observed weather~~

~~5~~ whereas temperature inversion concentrates pollutants in cold stable surface layers. The complex

5 interactions that lead to the observed weather patterns are challenging for Numerical Weather Prediction (NWP) models. To study the performance of the ~~COSMO-1 model anaylsis~~ COSMO-1E model analysis (KENDA-1), a measurement campaign took place from October 2021 to August 2022 in the 1.5 km wide Swiss Alpine valley called Haslital. A Microwave Radiometer and a Doppler Wind Lidar were installed at Meiringen, in addition to a multitude of automatic ground measurement stations ~~observing~~ recording meteorologic surface variables. Near the ~~measurement's~~ measurement sites, a low altitude pass, the Brünig Pass, ~~influence~~ influences the wind dynamic similarly to a

tributary.

~~The collected data shows frequent nighttime~~

~~10 temperature inversions for all months under study, which persist during daytime in colder months. An extended thermal wind system was also observed during the campaign, except in December and January allowing an extented analysis of along and cross valley winds. The comparison between the observations and the KENDA-1 data provides good model performances for monthly temperature and wind climatologies but frequent and important differences for particular cases, especially in case of foehn events. Modeled nighttime ground temperature overestimations are common due to missed temperature inversions~~

~~15~~ 10 The collected data shows frequent nighttime temperature inversions for all months under study, which persist during daytime in colder months. An extended thermal wind system was also observed during the campaign, except in December and January, allowing an extended analysis of along and cross valley winds. The comparison between the observations and the KENDA-1 data provides good model performances for monthly temperature and wind medians but frequent and important differences for single profiles, especially in case of particular events such as foehn. Modeled nighttime ground temperature overestimations are

15 common due to missed temperature inversions resulting in ~~bias up to 9~~ a bias up to 8 °C. Concerning the valley wind system, modeled flows are similar to the observations in their extent and strength, but suffer from a ~~to~~ too early morning transition time towards up valley winds. The findings of the present study allow to better understand the temperature distributions, the thermally driven wind system in a medium size valley, the interactions with tributary valley flows, as well as the performances and limitations of a model in such complex topography.

20 Keywords. Complex topography, Remote sensing, NWP, Temperature inversion, Valley winds, Foehn

~~20~~ 1 Introduction

Over mountainous areas, interactions between the terrain and the overlying atmosphere favor the ~~vertical transport of moisture and pollutants and consequently increase~~ horizontal and vertical transports of moisture and pollutants. The complex topography of the Alps consequently increases the air masses exchanges

~~between the boundary layer and the free troposphere.~~ 1

along the valleys and between the boundary layer and the free troposphere (De Wekker and Kossmann, 2015; Rotach et al., 25 2022). Both theoretical studies and experimental campaigns demonstrated that complex topography creates ~~circulation patterns with small~~

~~1~~

~~and large space and time pattern.~~ circulations with

small and large space and time pattern (Lehner and Rotach, 2018). In valleys, the superposition of the various processes leads to a complex vertical layering in the ~~25~~ mountainous boundary layer, which ~~is strongly related to the specific conditions of~~ strongly depends on the specific conditions of the surrounding terrain in each studied valley. For Numerical Weather Prediction (NWP) models, simulation of the atmosphere over complex terrain requires not only dense and accurate horizontal and vertical grids to ~~parametrize the mountainous terrain~~ parameterize the mountainous terrain

30 (Sekula et al., 2019) but also good estimates of vegetation, soil characteristics, net radiation, and speed of the large-scale flow (Adler et al., 2021). ~~1.1 Complex topography~~ Difficulties of models directly ~~the MWR/MEE T measurement. The maximal temporal T gradient usually follows sunrise and sunset (D~~

~~9~~

~~Fig. D1.a) with values up to ± 5 °C and remains below 1500 m~~ related to complex topography comprise among others the representation of ground-based temperature (T) inversions, of thermal valley winds and particularly of foehn events.

During calm clear nights, the air T in valleys can fall below the T measured across the surrounding hill tops leading to ~~high frequency of~~ cold-air pooling and associated T inversions in mountainous regions (Miró et al., ~~2018) (Joly~~ 2018; Joly and Richard, 2019). T inversions

35 influence fog formation ~~((Chachere and Pu, 2017)),~~ (Chachere and Pu, 2017), vertical dilution of pollutants ~~((Duine~~ (Duine et al., 2017; Diémoz et al., ~~2019)) and the development of the boundary layer during daytime ((Schnitzhofer et al., 2009)).~~ 2019) and the development of the boundary layer during daytime (Schnitzhofer et al., 2009). Such inversion are favored in ~~35~~ complex topography (Joly and Richard, 2018) and persists longer in deeper valleys, ~~where~~ whereas inversion lifetimes converge to the one over a plain for

wide valleys (Colette et al., 2003).

However, the small-scale nature of these near surface stable layers means that they are often poorly represented ~~in even the highest resolution operational NWP models ((Vosper et al., 2013)).~~ even in the 40 highest resolution operational NWP models (Vosper et al., 2013). The quality predictions for near surface variables during

stable conditions depends on locally generated circulations that are controlled by many factors such as turbulence, shortwave ~~40 and long wave~~ and longwave ~~radiation exceeds incoming shortwave radiation, a layer of cold air forms over all shaded colder surfaces. This air begins to move down the slope and converge in the valley floor, which stops up-valley winds and flips the flow direction. For~~ radiation, advection and subsidence. Deficiencies in the parametrization of the fluxes, ~~and especially during stable conditions have already been shown~~ especially during stable conditions, ~~which are captured by large grid~~

are well known (Hauge, 2006) and thus a finer grid resolution is needed in increasingly steep terrain (Sfyri et al., 2018). Simulations also ~~exhibit~~ underline the high sensitivity to the choice of the vertical grid in the prediction of cold pool formation

45 and suggest that the vertical resolution near the surface is more important than the height of the lowest level (Vosper et al., 2013). However, the assimilation of measurements, not only of surface data but also of profiling observations (Crezee et al., 2022), may improve the NWP performance for surface T inversions (Martinet et al., 2017).

~~(Nipen et al., 2020) even proposes to~~

~~integrate citizen observations (i.e. measurements from private meteorological stations) into NWP models. Future developments in these techniques may allow addressing the problem of T inversions.~~

~~1.1.2 Thermally induced valley winds and their interaction with synoptic flows~~

~~Thermally driven winds principally~~ Thermally driven winds primarily ~~on the climatology of measured MWR/MEE~~ occur under fair-weather conditions (Zardi and Whiteman, 2013). They develop due to ~~50~~ differential heating of adjacent air masses. They can partially be explained by the topographic amplification factor concept

50 (Whiteman, 1990) and ~~slope-flow-induced local subsidence in the valley center~~ local subsidence in the valley center induced by up-slope flow (Schmidli and Rotunno, 2010) leading to a faster heating of the ~~valley than of~~ air masses in the valley than over the plain. The valley–plain T contrast then produces an along-valley pressure gradient that induces strong ~~and deep~~ up-valley wind during the day and more shallow down-valley wind during the night. Slope winds are air mass movements parallel to the slope induced by buoyancy force in the presence of air layers at different T. Slope winds move upward ~~2~~

~~55~~ during the day and downward at night and play an important role in the morning and evening transition of

55 along valley winds. However, slope winds evolve over shorter time scales than valley winds (Serafin et al., 2018). The transition periods of up and down along valley winds are mostly driven by the sunrise and ~~sunset times.~~ sunset. Even though minor

changes in the topography can lead to a significant change in the flow regimes (Lang et al., 2015), some common features are observed among the existing studies. In general, the morning transition happens with a certain delay with respect to sunrise

caused by the time required for up slope winds and warm subsidence to erode the nocturnal T inversion. However, wind intensity ~~can be heavily related to tributary valleys (Zängl, 2004) and therefore highly depends on the local topography. As~~ 60 can be heavily related to tributary valleys (Zängl, 2004) and therefore highly depends on the local topography. In the evening, as

soon as the surface ~~outgoing~~ radiative balance becomes ~~significant for cold months (November-March).~~ negative, the cold air formed at the surface moves down the slope and converges in the valley floor, which reverses ~~more rapidly at sunset.~~

the flow direction from up-valley to down-valley winds.

Synoptic winds coupled with wind channeling effects can however superpose on the above described thermal mountain winds (Jacques-Coper et al., 2015). This large scale flows present no defined diurnal cycle and are generally stronger than the thermal

65 valley winds. Their effect on the valley wind system is highly variable and depends on the orientation of the synoptic flow with respect to the valley axis (Kossmann and Sturman, ~~2003). Finally, idealized simulations taking into account the interaction of the purely thermally driven flows with an overlying synoptic flow are rare (Rotach et al., 2015), so that further~~ 2003; Rotach et al., 2015).

The capability of mesoscale NWP models to calculate the above described diurnal valley winds in real valleys has been

investigated in a few studies (Chow et al., 2006; Langhans et al., 2013; ~~Schmidli et al., 2018; Schmidli and Quimbayo-Duarte, 2023). Globally, a good agreement between modeled and~~ Giovannini et al., 2017; Schmidli et al., 2018; Schmid et al., 2020; ~~Schmidli and Quimbayo-Duarte, 2023; Giovannini et al., 2017; Adler et al., 2021) in the Alps.~~

~~The campaign in the Haslital constitutes~~ Adler et al., 2021; Schmidli and Quimbayo-Duarte, 2023). Globally, a good agreement between modeled and

70 observed valley winds is achieved provided that spatial resolution of the models and surface data (e.g. snow cover and soil moisture) are high enough (Rotach et al., 2015). The size of the valley has ~~75 an impact on the accuracy of the modeled winds. Schmidli et al. (2018) showed that the COSMO1-E (resolution 1.1 km) diurnal cycle was well represented in large and medium valleys, but the valley wind speed is underestimated in smaller valleys. The same simulation with lower resolution of 2.2 km shows a larger tendency to diurnal wind speed underestimation.~~ an impact on the accuracy of the modeled winds (Schmidli et al., 2018). Generally, a closer agreement between the model and measurements was found for the smaller spatial resolution, which allows a better representation of the topography. (Wagner et al., 2014) shows that the grid resolution should be about 10 to 20 times smaller ~~80~~ than the relevant topographic scale to fully capture the different exchange processes. ~~With few exceptions, smaller altitude biases of the model at the ground result in reduced wind speed errors.~~ Hence,

75 increased grid resolution generally improves the performance of numerical simulations, which is even more pronounced if surface and soil model fields are accurately ~~initialized. Precise soil moisture data seems to be an important parameter to obtain good modeling results~~ initialized (Langhans et al., 2013; Schmidli and Quimbayo-Duarte, 2023).

Finally, the performance of models to handle foehn events had been shown to be ~~difficult. Operational analysis data from COSMO-1E exhibit~~ poor, with a cold bias over the whole profile bottom part (<1000 m) of valleys (Jansing et al., 2022; Tian et al., ~~2022). Wind speeds in the model are~~ 2022; Saigger and Gohm, 2022) and wind speeds generally higher, both above crest height and within the valley.

~~Modeling exercises reveal considerable differences in foehn occurrence frequency, which constraints the use of this data for studies at mesocale Saigger and Gohm (2022).~~

80 Although the surface measurement network is relatively well distributed over the Alps, T and wind profile measurements ~~via~~ by remote sensing (REM) instruments are rarely operationally performed in the Alpine valleys. However, a precise knowledge of the T structure of the atmosphere in complex terrain is essential for NWP models and the use of REM observations is a solution to obtain sufficient space/time resolution of the fast varying meteorological conditions in valleys.

~~Moreover few measurement~~

The campaign in the Haslital provides a unique set of observations including a long period of observation (ten months 85 comprising winter and summer months), a comprehensive measurement program with not only the MicroWave Radiometer

(MWR) and Doppler Wind Lidar (DWL) presented in this study, but also a ceilometer and a mobile X-band weather radar, a ~~100~~ location in a short, deep and moderately wide valley, that differs from most of the studies located in ~~long, wide valleys, and finally the presence of numerous ground stations in the Haslital or the auxiliary valleys to support the results.~~

~~The first objective of the campaign is to study the seasonal and diurnal cycles of T and wind in the vertical range containing the main topographical features (590-3000m). The analysis is focused on both climatology~~ long and wide valleys.

The first objective of the campaign is to study the seasonal and diurnal cycles of T and wind in the vertical range containing the main topographical features (590-3000 m a.s.l.). The analysis is focused on both seasonality and isolated events with a

90 ~~1.2 Goals of the paper~~

deepest interest on T inversion and foehn events. A comprehensive description of along and cross valley winds is performed, including a detailed analysis of thermal winds during a heatwave event at three stations along the valley and two grid cells of the model. The second objective is to evaluate the NWP model performance (KENDA-1) ~~for two model grid cells in the Haslital between the model's ground level and 3000m.~~ used in analysis mode in the Haslital.

Comparisons with the ground-based measurements and the profiling observations allow to assess KENDA-1 performance for both monthly ~~climatology and peculiar events.~~

averages and peculiar events.

95 ~~campaigns provided comparison of modeled and observed profiles of thermally induced winds system (Schmid~~ 2 Methods and Data

~~110 The campaign took place in Unterbach (MEE, a subsite in the Meiringen municipality) on the Haslital valley floor~~ The campaign took place in Unterbach (MEE), a secondary site in the Meiringen (MER) municipality in the Haslital valley
from October 13, 2021 to August 24, 2022 in so-called complex topography. ~~A MicroWave Radiometer (MWR) was measuring only since end of January whereas the Doppler Wind Lidar (DWL) and data from the NWP model are available during the whole campaign.~~
~~Both REM instruments sampled the entire winter and summer months.~~

The Doppler Wind Lidar (DWL) and data from
the NWP model are available during the whole campaign whereas the MicroWave Radiometer (MWR) was measuring only
since end of January, ensuring however observations during winter, spring and summer months (Fig. S1 for a global view of the

100 instrumental setup).
Unless otherwise stated, the following conventions are valid throughout the rest of the document: data are always reported by

the instrument or model name and the ~~site. E.g. MWR/MEE correspond to MWR measurements at MEE and KENDA-1/MER~~

site, e.g. MWR/MEE correspond to MWR measurements at MEE and KENDA-1/MER to
modeled data from KENDA-1 at the cell comprising MER site, altitude given in meters (m) is equivalent to the altitude above
sea level (m a.s.l.), wind speeds are given in km/h and direction in degrees according to north, ~~mentioned times are in UTC format, climatologies~~ times are in UTC format. Monthly

105 averages are aggregated according to the median hourly values of the studied parameter, median wind speed and direction are
calculated by vector averaging the hourly wind ~~vectors, KENDA-1 data refers~~ vectors.

2.1 Site

The observational site is located in Haslital, an alpine valley within the Swiss Alps in the Bernerse Oberland (Fig. 1). This 30
kilometer long valley extends from the ~~Grimselpass~~ Grimsel Pass (2164 m) to Lake Brienz (564 m). The upper ~~15 kilometers are~~ southern ~~foehn, a near systematic ground-T underestimation by both MWR (~0.2 to ~1.5 °C) and KENDA-1 (~2 to ~4 °C). Concerning the T profiles, KENDA-1 show a negative T bias between 2.5 and 4°C from the~~

15 kilometers are

110 oriented in the SE-NW direction and present a narrow valley floor with steep surrounding slopes. The Haslital is then joined by
a tributary valley called Gadmertal (NE-SW) and continues towards ~~NE~~ NW with a 1.5 km wide valley floor. About 5 km after
the junction, it is joined by the hanging narrow tributary valley of Rychenbachtal (SW-NE) at the Meiringen village. At this
point, the valley gradually bends from NW to ~~W and finally from W to~~ SW as it reaches Lake Brienz. Five ~~km~~ kilometers before the lake, the Brünig Pass
(1008 m) is an important topographic feature that connects the Haslital to the Sarneraatal, a 30 km long valley oriented in the

115 NE-SW direction ~~(B Fig. B1~~ (Fig. 1 presents a detailed map of the Sarneraatal and its connection to the Haslital). This pass interrupts the
near constant ridge's height ~~(around 2200 m) north to the valley longitudinal axis (B Fig. B2).~~

~~140~~

~~This study focuses on data from two particular sites. The measurements provide from both the in-situ SMN station at Meiringen village (MER) and the site of the REM campaign (MEE)~~ around 2200 m north to the valley longitudinal axis.

The campaign provides in-situ observations from the automatic Swiss Measurement ~~Techniques~~ Network SwissMetNet (SMN) station at
MER and REM observations from MEE facing the Brünig Pass. These two locations are separated by 4 km and are respectively
at 589 and 574 ~~m.a.s.l. The main difference~~ m a.s.l. The main differences between these two sites are the valley longitudinal axis angle (ϕMER = 300°,

120 ϕMEE = 270°) and the relative position to the surrounding connected valleys. Finally, the ~~KENDA-1 data are available for both sites according to the existing model 1.1 km grid.~~

~~The location of the 1.1 km grid cell in the 1.5 km wide valley has to be considered. Both used cells include part of the 150 valley~~ modelled data are available for both
sites according to the existing model 1.1 km grid.

Figure 1. a) Map of the geographical situation in the lower Haslital, b) along valley altitude of the valley floor (shadowed) and of the two crests and c) a detailed view of the campaign sites, the Brünig Pass and of the ground stations in the Sarneraatal. The automatic measurement from the SMN in Meiringen (MER) is represented in purple, blue and red, respectively. b) shows the differences between KENDA-1 and the RS. The height of the 3 main T inversions is also reported by dashed lines: bottom inversion at 08:30 (1760 m) and 11:00/14:00 (1560 m) and finally the upper inversion from 08:30 at 2920 m. c) T-profiles of RS in PAY at 12:00

Appendix F: RS 17.11.2021

48

Altitude [m.a.s.l.]
Altitude [m.a.s.l.] Altitude [m.a.s.l.]

Altitude [m.a.s.l.]

Figure G1. Monthly median wind direction [°] at ground level for the different automatic measurement station of the Haslital (top row) and Sarneraatal (bottom row). The color code is presented on the color wheel.

950 Appendix G: Wind pattern at SMN stations

All these stations show valley wind patterns from March to August and in November at some stations (MER, BRU, LUN and GIH). The up valley daily period at BRZ und BUC is less extended than few kilometers upstream in MER and LUN/GIH, respectively. This reduced time extents are probably due to the location of these stations near the slopes and not in the center of the valleys. The the campaign site in Unterbach (MEE) in red and the SMN station in Brienz in blue. The two cells of the model used are in pink. Up/Down valley Arrows representing up/down valley winds and slope winds are colored respectively in red/blue. ©swisstopo

6

The map was downloaded from Swisstopo (https://map.geo.admin.ch, last access: 12.01.2024)

2.2 NWP model COSMO/KENDA-1

The NWP model used in the study is the limited-area non-hydrostatic atmospheric model from the Consortium for Small-Scale Modeling Model (COSMO) (Baldauf et al., 2011) in the operational setup of MeteoSwiss. It uses a horizontal grid size of 1.1

125 are assimilated in every member using the km and 81 vertical levels with spacings from 20 m at the surface, 40 m at 1000 m, to 160 m at 3000 m and coarsening further up to the model top at 22 km. The levels are terrain-following and a smooth level vertical (SLEVE) coordinate transformation is applied (Leuenberger et al., 2010).

4

120 The operational COSMO The operational COSMO-1E forecasts are initialized by analyses produced by the Kilometre-scale Ensemble Data Assimilation system KENDA-1, similar to that described in Schraff et al. (2016), but using the above described model described in Schraff et al. (2016) and run in with the NWP setup of MeteoSwiss. Differences to the setup described in

130 Schraff et al. (2016) include the modeling domain (central Europe covering the Alpine Arc), the grid size of 1.1km and the observation errors tuned to the MeteoSwiss setup. KENDA-1 uses a 40 members ensemble of 1 hour model forecasts (first guess) and the following observations: SwissMetNet (SMN) ground station measurements (2m SMN ground station measurements (2 m a.g.l), surface T, humidity and surface pressure), aircraft observations (T and wind from AMDAR and MODE-S), radio soundings (T, humidity and wind), and radar wind profiler (wind). (wind

speeds > 25km/h). KENDA MEE and MER are similar

975 to the MWR measurements. For the rest of the profile, the model is again underestimating the T but higher up, between 1200 and 1400 m.

Appendix J: Wind speed and direction comparison during foehn

52

~~Figure J1. a)Wind direction comparison [°] and b) wind speed profiles comparison [km/h] timeseries between KENDA-1 MEE and DWL during a selection of 3 foehn events during the campaign: left 11-12.03.2022, middle 19-22.03.2022 and right 23-24.04.2022. Wind speed [km/h] and direction [°] from the SMN MER are given in the lower part of each figure.~~

~~53~~
5

speed and direction). In addition, radar-based estimates of surface precipitation are assimilated in every member using the
135 latent heat nudging method (Stephan et al., 2008). Model first guess and observations are combined using the Local Ensemble

Transform Kalman Filter (LETKF, Hunt et al., 2007) to obtain the best possible estimate of the current atmospheric state. The KENDA-1 analysis ensemble additionally uses lateral boundary condition perturbations and stochastic physics perturbations to optimize the spread-error relationship. Besides the ensemble analyses, a deterministic analysis member is calculated, which is close to the analysis ensemble mean (Schraff et al., 2016). ~~130 2.2~~ KENDA-1 data refer to the deterministic analysis member, which are

140 available in hourly time intervals but ~~corresponds~~ correspond to instant values.
Data from the two grid cells containing the MER and MEE stations were used. Both cells include part of the valley's north

slope, inducing ~~significant differences between the real topography and the model's terrain. The MER and MEE~~

~~cells present an offset of respectively 109 m and 130 m. This bias is not only observed in these two cells but in the whole study area. Indeed, the ridges and in particular~~ differences of 109 m and 130 m between the real topography and the model's terrain, respectively. The modeled
valley floor is globally raised by a hundred meters (Fig. ~~2).~~

~~5~~

~~Figure 1. Map of the geographical situation in the lower Haslital. The automatic measurement from the SMN in Meiringen (MER) is represented in yellow, the campaign site in Unterbach (MEE) in purple.~~ S2), whereas the ridges and the Brünig Pass are lowered with respect to their real ~~altitudes, whereas the~~ altitudes. The altitude difference between the valley floor and the crests is thus reduced of several hundred meters and,

145 in particularly, the Brünig Pass is only 200 m higher than the valley floor.

2.3 Instrumentation

2.3.1 ~~SwissMetNet station MER~~

~~The ground measurements in MER are part of the automatic measurement network (SMN) operated by MeteoSwiss (in yellow on fig.1). It~~ In-situ meteorological data

The ground measurements in MER are part SMN operated by MeteoSwiss and provide every 10 minutes near real time data of T, humidity, surface ~~pressure) measured~~

pressure, precipitation amount, wind speed (mean and gust) and ~~direction (10~~ direction, global radiation, sunshine

150 duration, snow height and an operational foehn ~~index(Dürr,~~ index (Dürr, 2008). Surface pressure, T and relative humidity observations of the MER station are actively assimilated in KENDA-1. Anyhow, the observations considered as too far from the modeled data are rejected during the assimilation phase, so that a comparison between the observed and modeled data at MER allows making ~~extensive climatologies. The SMN data are composed of T and humidity~~ assumption on the models' skills. SMN also contains a station in Brienz (BRZ) and in the Sarneraatal (Fig. 1) in the locality
of Giswil (GIH). This allows for assessing the influence of the winds originating from this auxiliary valley. MeteoSwiss also

155 cooperates closely Federal Roads Office (FEDRO) that ~~operates its measurement networks. Wind measurements from the Brünigpass~~ also operates wind measurements at the Brünig Pass (BRU), Lungern
(LUN) and Buchholzbrücke (BUC) ~~are therefore also at disposal~~ with similar temporal resolution.

2.3.2 ~~Additional ground observations in Sarneraatal~~

~~SMN also contains a station in Brienz (BRZ) and in the Sarneraatal (B)~~ Microwave Radiometer

A MWR (HATPRO-G5 produced by RPG Radiometer Physics Gmbh) is used to obtain T profiles ~~and the related mixing layer heights. It collects~~ by collecting microwave
radiation to infer the T (Rose et al., 2005). It performs a scan every 5 minutes at 11 elevation ~~7~~

angles and operates in 14

160 frequencies reception bands in two regions: 22-31 GHz (7 channel filter bank humidity profiler and LWP radiometer) and 51-58 GHz (7 channel filter bank T profiler). The device has an optical resolution of 3.5° (half power beam width) at 22 GHz. The data acquired during rainy conditions are discarded. The ~~spatial vertical resolution increases from 50 m at 250 m.a.g.l. to 300 m at 2500 m.a.g.l. (C)~~ radiometer is measuring from 50 m above ground to 2500 m, the first MWR level is then at 625 m. The spatial vertical resolution increases from 50 m at the bottom to 300 m at the top and corresponds to a related T accuracy between 0.25 °C to 1.00 °C, ~~respectively.~~ ~~Löhnert and Maier (2012) found an RMSE between~~ respectively (Tab. S1). Löhnert and Maier (2012) found an RMSE between

165 retrieved profiles and radiosonde data between 0.4 and 0.8 K in the lowest 500 m a.g.l., within 1.2 K at 1200 m and around 1.7

6

K at 4000 m above ground. However, the performance of an MWR is highly related to the retrieval algorithm and the ~~data used to train the latter (Rotach et al., 2015).~~

~~The MWR indirect measurement and the trained retrieval algorithm~~ training dataset (Rotach et al., 2015). During the Meiringen campaign, the retrieval of Payerne was used (Lohnert and Maier, 2012). This retrieval uses Payerne's radiosonde data to perform the multi-linear regression leading to potential further uncertainties. The instrument at MER had a line of sight of about 10 km inducing no further additional uncertainty due to obstacles of the

~~surrounding terrain in the line of sight can be a source of external~~ 170 ~~angles and operates in 14~~ surrounding terrain (Löhnert et al., 2022). In simple topography, Hervo et al. (2021) showed that the HATPRO-G5 can be still biased when compared to radio soundings with a cold bias of 0.5 K around 1500 m altitude.

~~2.3.4 Doppler Wind Lidar (DWL)~~

2.3.3 Doppler Wind Lidar

DWL can be used to infer wind speeds and direction even in complex topography (Wang et al., 2016). During the campaign, a Vaisala Leosphere Windcube 100S DWL was deployed in MEE to measure wind speeds with a vertical resolution of 100 m. In

175 ~~500 m.a.g.l., within 1.2 K at 1200 m and around 1.7~~ the used measurement mode, 120 second zenith scans ~~performed each 10 min to measure vertical wind speed, Range Height Indicator (RHI) scans to measure~~ were performed each 10 min to measure vertical wind speed and Doppler Beam Switching ~~(DBS)~~ scans providing 7 independent wind profiles every 5 min ~~to measured horizontal wind speed. In this analysis the wind profiles were averaged for each 5 minutes interval.~~ from 200 m to 12000 m above ground, the first DWL level is then at 775 m. Data collected during rain events or/and with confidence level < 90% are discarded. Moreover, data with wind speeds lower than 2 km/h were discarded for the wind direction analysis. The data availability during the entire campaign is of 80 % at 1000 m a.g.l. and 50% at 2500 m a.g.l.

180 ~~of sight of about 10 km should not induce further additional T uncertainty.~~ 3 Results

~~In this section, the measurements of T and wind in the Haslital and its surroundings are presented. The measured climatology for T (6 months) and winds (10 months) is analyzed and then compared to KENDA-1 outcomes. Special cases are treated with particular attention such as surface based T inversion, valley winds and foehn events.~~

~~3.1 Temperature~~

The measurement campaign at Meiringen allows a detailed description of the seasonality of the six months T and 10 months wind observations in the Haslital and its surroundings. Profile observations were performed at MEE and surface in-situ observations at MER, whereas the modeled surface and profile data are available at both sites. For both the T (sect. 3.1) and the wind speed and direction (sect. 3.2), the seasonality of the profile's ~~evolution during inversion in winter and summer are available in the appendix (E). The amplitude of the KENDA-1/MEE ground T overestimation is proportional to the amplitude of the T inversion.~~

~~14~~

~~As the amplitudes of T inversions are more pronounced during cold months than in summer (Fig. 7.b), March exhibits the most extreme values of ground T differences. It has to be noted that no systematic differences are observed between KENDA-1 T over MEE and MER.~~

~~NOV DEC JAN FEB MAR~~

~~a) 100 100 100 100 100~~
~~Station~~
~~KENDA~~

~~50 MWR 50 50 50 50~~

~~0 0 0 0 0~~
~~0 10 20 0 10 20 0 10 20 0 10 20 0 10 20~~

~~APR MAY JUN JUL AUG~~
~~100 100 100 100 100~~

~~50 50 50 50 50~~

~~0 0 0 0 0~~
~~0 10 20 0 10 20 0 10 20 0 10 20 0 10 20~~

~~NOV DEC JAN FEB MAR~~

~~b) 6 6 6 6 6~~

~~4 4 4 4 4~~

~~2 2 2 2 2~~

~~0 0 0 0 0~~
~~0 10 20 0 10 20 0 10 20 0 10 20 0 10 20~~

~~APR MAY JUN JUL AUG~~
~~6 6 6 6 6~~

~~4 4 4 4 4~~

~~2 2 2 2 2~~

~~0 0 0 0 0~~
~~0 10 20 0 10 20 0 10 20 0 10 20 0 10 20~~

~~Time of the day~~

observations and the model's performances at MEE are first described.

185 ~~There are three measurement modes:~~ Surface observations are than used to study specifically surface based T inversions and heterogeneity of the winds in the Haslital
valley. Even if SNM/MER surface observations are assimilated by KENDA-1, the comparison of the modeled and observed data
allows evaluating the impact of the assimilation at MER. Finally, a last section describes ~~the differences between the MWR/MEE retrieved T profiles and KENDA-1/MEE modelled~~
~~T between 705 and 2500 m.~~

Kenda-1 performances in case of foehn
events.

During the campaign, the mean T was 1°C below the 1991-2000 norm in December and January but clearly above the norm
190 ~~2500 m a.g.l.~~

~~2.3.5 Radio-sounding~~

~~The radio-sounding on the 17.11.2022 were performed by a Vaisala RS41, which is a compact lightweight sonde measuring T,~~
~~wind and humidity profiles with a vertical resolution of 5 m. The three~~ (1.5 to 2.5°C) in February, March and from May to August. Three ~~events have been selected~~
~~(10.03-16.03/19.03-22.03/26.06-27.06) corresponding to~~ heat waves occurred, the first one lasting 6 days in mid-June,

the second lasting 4 days around mid-July ~~(4 days). Finally, a third heat~~

and the third one reached Switzerland at the beginning of August. Snow cover and
precipitation are important parameters since the surface albedo and the soil moisture affect the development of cold pools with T
inversion, subsidence, the atmospheric boundary layer development and consequently thermal valley winds. Only 60% of the
precipitation of the 1991-2000 norm were observed in November, but 120% in December. ~~These precipitations arrived in form of snow end of November~~

(25 cm of fresh snow) and continued during the first half of December leading to a total snow cover of 40 cm the 15.12.2021. Snow covers the valley's floor from

195 2.4 Weather situation during the campaign

During November and December, standard sunshine duration values were recorded, but with only 60% of the precipitation of the 1991-2000 norm in November and the end of November to mid-December. Heavy precipitation occurred then at the end of the month with a snowfall limit recorded at about 2500 m. Consequently, snow

200 cover remained below the 15 cm mark until the end of the winter. January, February and March were particularly sunny with

strong reduced then the snow cover to less than 15 cm until the end of the winter. Strong precipitation deficits happened in January and especially in March (35 and 15 mm). March experienced frequent foehn events (95 hr determined from the MeteoSwiss foehn index). In April, the weather was changing, with 8 cm of snow precipitation the 01.04. The months from May to August were extremely mild and precipitations were 50% or index (Dürr, 2008)). Precipitation from May to August was 50% or

less compared to the norm, except for June (96%). The first heat wave (6 days) started in mid-June and the second came full evolution of T, precipitation and sunshine duration is aggregated in the supplement (Tab. S2 and Fig. S3) and the wind features are fully described in the results section.

200 3.1 Temperature

3.1.1 Climatology

This section focuses Seasonality of temperature profiles at MEE

The evolution of T in MEE from February to July (Fig. 2.a) presents as expected clear diurnal cycle with a vertical extent depending on the season. Layer with higher T develops gradually from sunset to sunrise to reach monthly-related maximal T and height. This layer of warmer air persists during the first half of the night and then gradually fades out towards sunrise.

205 wave reached Switzerland at the beginning of August. The full evolution of T, precipitation and sunshine duration is aggregated in table A1 and Fig. A1 from A.

2.5 Conventions

The time of the T maximum, the persistence of the warm layer and the T range between ground and 2500 m are all enhanced during summer months. Between the mean ridge height and 2500 m, the T remains however relatively constant throughout the day in winter (February). This thermal cycle presents a T rise shortly at sunset from March on, but especially in April and May. This artifact could be caused by the MWR/MEE measurement axis pointed towards West, so that sunshine with low angle at sunset

The maximal temporal T gradient usually follows sunrise and sunset (Fig. S4) with values up to ± 5 °C/km confined below 1500 m in the morning whereas vertical negative gradients between -4 and -6.5 °C/km (D-D1.b) are coherent with standard values (Lute and Abatzoglou, 2021).

A thermal inversion layer is particularly visible from midnight to sunrise (Fig. 3.a are observed in the evening.

In May and June, underestimations are constrained to nighttime and more important between 700 m and 1500 m. July also exhibits lower altitude (< 1000 m) T underestimation from noon to midnight but also a near-continuous T underestimation at ridge level. The latter was, to a smaller extent, already present in June in the afternoon. MWR/MEE and KENDA-1/MEE Ts are however similar between these two underestimated T layers. KENDA-1/MEE mean monthly climatology present lightly lower T than the MWR/MEE T profile with differences

210 A thermal inversion layer is particularly visible from midnight to sunrise (Fig. 2.a) for all months in the study. The frequency of occurrence of these T inversions are highlighted by the positive vertical T gradient (D-D1.b) near near the ground (590-1000 m).

m) for all months in the study. The frequency of occurrence of these T inversions are highlighted by the positive vertical T gradient. A complete analysis of T inversion will be described in section 3.1.4.

3.1.3.

~~The bias during the day can be~~
~~partially explained by the altitude difference between the real topography and the DEM of KENDA-1 since the median T~~

Fig. 2.b presents the differences between the observed MWR/MEE and modeled KENDA-1/MEE T profiles. The main observed pattern is a general low altitude (< 1500 m) T underestimation from KENDA-1/MEE. In February, this underestimation

215 lasts almost the whole day up to 2500 m, but is larger (< -1 °C) below 1500 m. March and April exhibits the same T underestimation below 1500 m, while a small T overestimation (< 1 °C) is also observed in March over the ridges in the morning. In May and June, underestimations are constrained to nighttime. July also exhibits lower altitude (< 1000 m) T underestimation but also a near continuous T underestimation of up to -2°C at ridge level, that was already partly present in May and June. The 1-2°C underestimations of KENDA-1/MEE models are then slightly larger than the MWR uncertainties comprised between

220 0.25 and 1°C as a function of altitude (see sect. 2.3.2). The cold bias between the MWR and the radio sounding ~~were launched the MEE site at 08:30, 11:00~~
~~and 14:00 UTC.~~

could however
suggests a larger error of KENDA-1.

3.1.2 Surface ~~Temperature comparison~~

~~In this section, the MWR/MEE ground T at MEE and KENDA-1 ground T at MEE and MER are compared to the measurements at the MER SMN station, used as a reference.~~

temperature comparisons

To better estimate the reliability of the REM observations and of the model, the first levels of MWR/MEE, KENDA-1/MEE and KENDA-1/MER are compared to the SMN/MER measurements used as a reference due to its low uncertainty (≈ 0.2 ~~°C) and can therefore be considered as the reference~~
~~for the comparison with KENDA-1 ground T and MWR/MEE measurements at the first level. The distribution of T differences between MWR/MEE in MEE and the SMN station in MER (Fig. 4.a) is~~ °C).

225 ~~and height. This layer of warmer air persists during the beginning~~ The T differences between MWR/MEE and SMN/MER (Fig. 3.a) are normally distributed with mean and median close to zero
(-0.07°C) and RMSE equal to ~~1.45 °C. Extreme values~~ 1.45°C. Extreme differences (3σ) ~~correspond to differences~~ are larger than ± 4.35 °C.

The distribution of ground T differences between KENDA-1/MEE and SMN/MER (Fig. ~~4.b)~~ 3.b) is wider than for the MWR/MEE (RMSE = 2.23 °C) and exhibits a positive skew (median = -0.27 °C and mean = +0.03 °C). Extreme values are significantly more frequent than for the MWR/MEE measurements, especially in the positive part of the distribution. KENDA-1/MEE T

Figure 2. ~~COSMO-1 altitude bias [m] relative to the 25 m resolution digital elevation model in the region of~~ a) Monthly diurnal cycle of MWR/MEE T from February to July 2022. Monthly scales with a range of 20 °C but with minimum T based on the MWR/MEE profiles are used. b) Diurnal cycle of the median T profiles difference [°C] between KENDA-1/MEE and MWR/MEE for each month. The dashed vertical lines correspond to sunrise and sunset times and the dashed horizontal line to mean ridges' height.

230 ~~might perturb~~ underestimations occur more often but with lower absolute differences than overestimations, ~~whose differences with the SMN/MER T reference can reach up to 9 °C. A similar distribution is observed for KENDA-1/MER (Fig. 4.c) with the same occurrence of~~ and differences with the SMN/MER
T reference can reach up to 9 °C. A similar distribution is observed for KENDA-1/MER (Fig. 3.c) with the same occurrence of

Figure 3. ~~a) MWR/MEE T climatology b) KENDA-1/MEE T climatology from February to July 2022 between 590 and 2500 m. Monthly scales with a range of 20 °C but with minimum T based on the MWR/MEE profiles are used.~~

Distribution of the ground hourly T differences for a) MWR/MEE-SMN/MER b) KENDA-1/MEE-SMN/MER, c) ~~KENDA/MER-SMN/MER.~~ KENDA/MER-
SMN/MER. The gray distributions are the ground T differences with ELR corrections. ~~KENDA-1/MER and KENDA-1/MEE during most of the cycle. The differences induced by T inversion during nighttime are the~~

same. The modeled ground T in the cell over MER shows however smaller differences during daytime, The dotted and dashed lines correspond to the median
and the mean, respectively.

extreme T differences (217 hr). Differences under 2 °C represent 71.1 % at MER and 66.0 % at MEE which 250 explains the slightly smaller RMSE for the cell over the SMN station.

To check if the altitude differences of respectively 130 and 109 m between the real topography and KENDA-1 ground

level height at MEE and MER could explain the T differences with the SMN station, between the stations and KENDA-1 first levels could explain the T differences with
235 In winter, not only nighttime but also daytime near ground T inversions are measured, but they are rare from March apart. SMN/MER, a standard T correction with a mean environmental lapse rate (ELR) of -5.25 °C/km (Lute and Abatzoglou, 2021) is applied. This mean ELR is close to the mean
measured MWR/MEE lapse rate of -4.59 °C/km between 590 and 740 m. The distribution of T differences after this correction

(-6.5 °C/km (Lute and Abatzoglou, 2021))

close to the mean measured MWR/MEE lapse rate (-4.59 °C/km between 590 and 740 m) was applied to the modeled profiles. Considering the remaining T differences after the correction (grey in Fig 4.b and 4.c) shifts to higher values leading to a higher mean difference, the right-skewness and standard deviation
being however conserved. The correction leads to higher RMSE at both stations and consequently to a global worse agreement between the SMN and the model T. The difference in the effect of the ELR correction between MEE and MER is probably linked to the assimilation of MER measurements by KENDA-1. This type of correction is valid when a large number of values accounting for various meteorological conditions are aggregated. It is consequently not precise in specific cases (e.g. T inversion),

3.b and 3.c), we conclude that the horizontal and
vertical distances between the SMN station and the first level of profiles over MEE are not the main causes of KENDA-1 discrepancies in ground T estimation.

The T differences between KENDA-1/MEE, KENDA-1/MER, MWR/MEE T and SMN/MER T (Fig. 5) shows a clear diurnal
SMN/MER station and the first level of KENDA-1/MEE are not the main causes of discrepancies
in ground T estimation.

240 Ground T measurements from the SMN have a The median diurnal cycle of T differences with SMN/MER T (Fig. 4) shows that KENDA-1 overestimates the T during
nighttime (+1.5°C) in both cells and underestimates it during the day (-2°C in MEE and -1.5°C in MER). The interquartile range (0 to 3.5 °C) and the whiskers (-4 to 8 °C) of the differences are larger during the second part of the night for KENDA-1 when surface T inversions are more frequent. The presence of this phenomenon strongly influences the amplitude of the differences and is detailed in the next section (see details in next section 3.1.3), One must be aware that the KENDA-
third of the daily bias can be explained by the altitude difference between the

245 station and the KENDA-1 first level since the median T correction during daytime is around 0.65°C. The T bias distribution of KENDA-1/MER and KENDA-1/MEE are similar during most of the cycle. The modeled daytime T over MER shows however smaller differences to SMN/MER than over MEE, which can be explained by the reduced altitude bias or the reinforced assimilation. MWR/MEE also follows a similar cycle with a negative T bias (min. of -1 °C) has a negative T bias (> -1°C) from 6:00 to 15:00. A slight overestimation is present 15:00 followed by a slight overestimation from 15:00 to 21:00 (max. of + 0.5 °C). The MWR/MEE T

(< + 0.5 °C). The MWR/MEE T differences present smaller whiskers and interquartile range during the second part of

250 the night than KENDA-1/MEE, but they are similar during daytime. Globally, the measured MWR/MEE first level T are closer to the SMN/MER T than the modeled T.

10

Figure 4. Ground T differences distribution Box plots and whiskers of hourly ground T differences between the SMN/MER and the MWR/MEE (blue), the SMN/MER and
KENDA-1/MEE (red), the SMN/MER and KENDA-1/MER (pink) as a function of daytime. The dashed lines represent the median of the distributions.

3.1.3 T profile comparison

The T profile comparisons Surface temperature inversion

A comparison between the T inversions detected by KENDA-1/MEE cell
overlaping the south facing slope (Fig. 1) than by the DWL/MEE located in the middle of the valley. Fig. 13.a shows the mean two ground observations at different altitudes (MER and BRU

stations), MWR/MEE profiles and KENDA-1/MEE T.

The analysis of the T profile climatology (Fig. 3), the ground T (Fig. 5) and the T profile differences (Fig. 6) show that
BRU), by REM
MWR/MEE and modeled by KENDA-1/MEE allows a better estimation of the frequency of occurrence of cold pools, the

255 sensitivity of REM observations and the limitations of the model.
The analysis of the negative ground T difference between MER at 590 m and BRU at 998 m (horizontal distance = 3.7 km)

shows that near ground T inversions are common during the night for all months in the study (Fig. 5.a). Their frequency is
60% in December and January (all day long), 40% during the night in spring and 30% during the night in summer. spring nights and 30% during summer nights. Daytime near ground
inversions are rare from March apart onwards and common between November and February (20-60%). The observed T difference follows a seasonal cycle with

300 enhanced amplitude during winter months reaching up to 4 °C (Fig. 7.b). inversion

260 not applicable to the whole profile and is therefore not further applied in this study. Considering the presented differences between the SMN and KENDA-1 T as a function of grid cell and ELR correction, amplitude follows a seasonal cycle with stronger inversions during winter months reaching up to 4 °C (Fig. 5.b). In summer, this
amplitude is reduced to about 2°C and constrained to nighttime. The erosion speed of the T inversion is independent of the month. However, the delay of the erosion onset to sunrise is smaller in summer.

The same analysis between these summer (about 2h) than in winter (about 4h).

The same analysis between two similar elevations is performed on MWR/MEE and KENDA-1/MEE T profiles. MWR/MEE shows higher frequencies of T inversion than both the ground stations and KENDA-1/MEE, especially for June and July.

265 cycle. MWR/MEE also presents a larger amplitude of the T inversion than the ground observations and KENDA-1/MEE with maximum difference of +2°C and +4°C, respectively. Even if the capability for KENDA-1/MEE to detect the near ground T inversions is enhanced from November to January, their amplitude is always underestimated by 1-2°C (Fig. 5.b). Moreover, from May to August, the presence of T inversion in the first hours after sunrise is also underestimated by KENDA-1/MEE, which can impact the onset time of up valley winds (section 3.2.2). All this leads to both an important
overestimation of the T at ground level (Fig. 5) and a slight underestimation of the T just above the T inversion (Fig. 6). To

The missed T inversions by KENDA-1/MEE leads to both its important

270 correction is around +0.65 °C during daytime, reducing the difference by a third. The T difference distribution is similar between

overestimation of the T at ground level (Fig. 4) and its slight T underestimation between 850-1200 m (Fig. S5 for detailed examples).

Figure 5. Box plots and whiskers of ground T differences between the SMN/MER and the MWR/MEE (blue), the SMN/MERn and KENDA-1/MEE (red), the SMN/MER and KENDA-1/MER (pink) as a function of daytime. The dashed lines represent the median of the different
a) Diurnal cycle of the hourly T inversion frequency between T at SMN/MER (589 m) and FEDRO/BRU (998 m) ground stations, at the lowest level (640 and 705 m, respectively) and 1000 m of MWR/MEE and KENDA-1/MEE profiles. The 1D measured values were interpolated using a linear interpolation with 10 m spaced vectors. b) Mean ΔT for the time where an inversion is detected. Sunrise and sunset are represented by the dotted lines

dotted lines.

The analysis of the assimilation process for nights with strong ground KENDA-1 KENDA-1/MER T overestimations shows that the model suffers from a systematic deficiency. During these nights, differences between the model's first guess and observations are mainly around 5 °C and can reach 10 °C in extreme cases (results not shown), so that observations are rejected due to differences

275 differences present smaller whiskers and interquartile range during the second part of the night than KENDA-1/MEE, but, during daytime, they are similar. Globally, the MWR/MEE first level T are closer to the SMN/MER T than the modeled T.

exceeding the predefined ~~threshold. The ensemble first guess and~~ threshold based on the ensemble first guess, its spread ~~as well as the observation error, that is assigned to 2 m temperature observation are the main causes of the assimilation or not of the values (T,~~ and the observation error. ~~The instrument at MER was scanning in the west (275°) direction parallel to the Haslital so that the line~~

During these periods,
the ~~SMN T at MER is therefore not assimilated by the model analysis (KENDA-1).~~ SMN/MER T is therefore not assimilated by the model analysis.
Even if the observations are assimilated for some of the
KENDA-1 time steps, the assimilation has a very limited effect and allows only minor corrections towards the observations (<
1 °C) during some nights in both MEE and MER. ~~3.1.5 Cloud-topped inversion~~

~~A T inversion at higher altitudes was measured on the 17th of November~~ It has to be noted that the KENDA-1 T overestimation during nighttime is similar at MEE and MER (Fig. 4).

280 ~~The main pattern observed across the different months (Fig. 6) is a general low altitude (< 1500 m) T underestimation from KENDA-1/MEE. In February, this underestimation lasts almost the whole day up to 2500 m, but is larger (< -1 °C) up to 1200-1600 m and below 1 °C difference at higher altitudes. March exhibits the same T underestimation but it is constrained from 15:00 to 05:00 to the lower part of the profile. The underestimation is larger (< -2°C) in the first part of the night due to marked T inversion (section ?? and D). A small T overestimation (< 1 °C) is also observed over the ridges in the morning.~~

3.2 Wind

During the campaign, wind profiles were measured at MEE by the DWL, whereas ground based 10 m wind compounds ~~were analyzed at the SMN/FEDRO station in MER, BRZ and in the Sarneraatal (BRU, LUN, BUC and GIH). Complete wind profiles (0-3000 m) were only measured at MEE. KENDA-1 profiles are extracted and analyzed over MEE and MER. It is important to take the orientation of the different valleys or valleys' sections into account when analyzing the wind directions at the different stations, especially for the Haslital that bends between~~

are
constantly measured at MER and at five other SMN or FEDRO ground stations (Fig. 1). Modeled wind profiles from the two grid cells of MER and MEE are further used. The average measured wind profiles' seasonality is first described followed by a more detailed analysis of the along and across valley components at MEE. The performance of KENDA-1/MEE is analyzed

12

285 ~~The T underestimation of April extends from midday to late~~ in each section. A comparison between the results in MEE and in other ground stations in the valley gives an insight in the
complexity of the ~~atmosphere itself, which can be composed of several layers with thermal structures and wind regimes inducing enhanced mass~~

wind system caused by the peculiarities of the valley's topography.

3.2.1 ~~Climatology~~

Seasonality of wind profiles at MEE

For the monthly average of DWL/MEE and KENDA-1/MEE profiles, wind directions are split into two speed categories, below
and above 20 km/h, to distinguish between thermally induced valley winds and external synoptic winds, respectively. Fig. ~~8.a presents the monthly mean wind directions from the DWL/MEE observations at MEE. A clear distinction between winter months (DJF) and the rest of the campaign period is observed:~~

6.a

290 ~~rarely exceeding -2°C.~~

presents the monthly mean wind directions from the DWL/MEE observations.
Concerning thermally induced winds (ws < 20 km/h), winter months do not show a clear presence of regular direction

changes at any altitudes. A predominance of ~~east winds is measured in February and January at low altitudes.~~

~~– During March, even though the winds > 20 km/h are mainly~~ easterly winds is measured in January and February at low altitudes. During March, despite the channeled ~~E~~ easterly winds due to frequent foehn events, the formation of valley winds pattern is already clearly visible.
Their time extent ~~(from~~ from mid-day to ~~sunset) and vertical extent (up to 1500 m) is similar to November.~~

~~350 – The formation of thermally induced wind is principally visible from April to August (ws < 20 km/h). A classical valley wind pattern is observed at MEE with a simultaneous (for summer months) up valley wind onset and a gradual onset of down valley wind triggered from the ground up to the ridge's height.~~ sunset is similar to November. The formation of thermally induced wind is

clearly visible

295 ~~important differences are more common in the presence of T inversion. The analysis of the negative ground T difference between~~

~~the MER station at 590 m and the BRU station~~ from April to August (ws < 20 km/h) and will be further discussed in the next section (3.2.2). From 10:00 to mid-afternoon, the
direction at low altitudes (800-1000 m) is mainly from W-SW, whereas flows from W-NW are measured in the rest of the profile
concerned by up valley winds (see further explanation in sect. 3.3). Synoptic winds (ws > 20 km/h in Fig. 6.a) are measured
between 2000 and 3000 m from W-SW direction for all months, with a higher variability in ~~January. In December and February, high winds from W-NW are prevalent below 1500 m~~
~~whereas various directions from N to SE directions are observed for the others months.~~

January and a strong influence of
foehn events up to 2500 m in March. In December and February, high speed winds from W-NW are prevalent below 1500 m

300 whereas various directions from N to SE directions are observed for the others months. From April to November, high speed N
winds from Sarneraatal (sect. 3.2.3) are also observed from the ground to 1000-1500 m from the late morning to several hours
after sunset.

Figure 6. ~~Diurnal cycle of the median T profiles difference [°C] between KENDA-1/MEE and MWR/MEE for each month. Sunrise and sunset are given by the dashed lines.~~

~~3.1.4 Surface T inversion~~

~~For the frequency and amplitude comparisons of the T inversions, the data used are ground observations~~ Monthly median wind direction [°] for a) DWL/MEE, b) KENDA-1/MEE and c) KENDA-1/MER (01.11.2021-23.08.2022). In each
case, the data are split according to the threshold wind speed of 20 km/h.

KENDA-1/MEE wind profiles (Fig. 6.b) are generally very similar to the DWL/MEE observations. The good KENDA-1/MEE
performances comprise first the influence of the foehn up to 2500 m (ws > 20 km/h) as well as the presence of valley wind below

305 ~~July. For T amplitude, the maximum difference is relatively constant with ground observation and the model, respectively + 2 °C and + 4 °C. Even if the capability for KENDA-1/MEE to detect the near ground T inversions is enhanced from November to January, their amplitude is always underestimated (Fig. 7.b). Moreover, for March, May and August, the frequency decreases too rapidly after sunrise~~ 1200 m (ws < 20 km/h) in March. Second, the synoptic wind flows (ws > 20 km/h) captured by large grid model inputs and by assimilated measurements ~~(RS, MWR/MEE/DWL/MEE profiles, ...) from the Swiss plateau.~~

~~The wind by KENDA-1 at MER is very similar to the results at MEE (Fig. 8.c) taking into account the different orientation of the valley at both stations. In March, the influence of up valley winds is more pronounced in MER with a clear extension up to 2000 m. For the warmer months, the thermally induced wind diurnal cycle is more pronounced and presents with some new patterns. The onset of up valley winds is even more delayed up to higher altitude~~ (e.g. RS, MWR and DWL profiles) from the Swiss plateau are consequently very well modeled.
Finally, the main valley wind patterns in November and from March onwards are well represented by KENDA-1/MEE. Apart
from inaccuracies related to the valley wind transitions (see 3.2.2), the model and the measurements differs in the presence
of frequent N flows from the Brünig Pass between the ground and 900-1200 m with increasing frequency towards sunset in

310 ~~further illustrate this phenomenon, two full~~ KENDA-1/MEE, whereas N flows are rather found at higher altitude (1300-1700 m) in ~~the measurements.~~

~~– The influence of the foehn up to 2500 m (ws > 20 km/h) as well as the presence of valley wind below 1200 m (ws < 20 km/h) in March are both well modelled by KENDA-1/MEE.~~

~~– For winds above 20 km/h, the match between DWL/MEE observations and KENDA-1/MEE is almost perfect. These flows are more easily modeled since they are mainly influenced by synoptic~~ DWL/MEE. This feature is mostly
caused by the KENDA-1/MEE cell overlapping the slope towards the Brünig Pass so that winds at the junction between Haslital
and Sarneraatal can influence the median modeled wind compounds. ~~The comparison between KENDA-1/MEE and the DWL/MEE observations leads to the further conclusions:~~

~~–~~Finally, during winter months, KENDA-1/MEE models
continuous down valley (E) winds (ws < 20 km/h) ~~from December to February between ground and 1000 m. These down valley winds are however not observed by the DWL/MEE in December.~~

between ground and 1000 m that are less continuously ~~measures the main meteorological variables since 1889 and provides near real-time data every 10 minutes~~
~~since November 2011, which allows for~~ observed by the
DWL/MEE in January and February and even absent in December.

315 3.2.2 ~~Valley winds~~

~~To extend the wind analysis, the data from the SMN/MER station, the DWL/MEE and KENDA-1 at MEE and MER, relative to speed and~~ Along valley winds

To extend the wind analysis, the data from the SMN/MER station, the DWL/MEE and KENDA-1 at MEE and MER are
transformed according to the valley longitudinal axis directions at ~~MER and MEE.~~

both sites. For this analysis, the positive wind speeds (red
color) correspond to up valley wind (Fig. 1) and to northern wind from the Brünig Pass for along and across valley winds,
respectively, and negative wind speeds (blue color) to opposite directions.

320 ~~at the surface.~~ Fig. 7.a shows the diurnal and seasonal cycles of the along valley wind speed at SMN/MER during the campaign. The
occurrence of along valley winds is confirmed by the ~~clear diurnal~~

~~cycle from February to November. A constant 4 hours delay between sunrise and the onset of up valley winds (> 10 km/h) is observed in the 10-y climatology whereas this delay decreases to 3.5 hours in the summer months 2022 during the campaign. February 2022~~ diurnal cycle in November and from February to August. A 3-4 hours
delay between sunrise and the onset of up valley winds (> 10 km/h) is observed. February shows some early up valley wind
but their origin is more linked to synoptic flow intrusions. The transition to down valley winds ~~is closely related to sunset and exhibits a maximum delay of 1 hour in the climatology. In 2022, it occurs 1~~

~~400 hours before sunset in March and June, at sunset in April and May, July and less than hour after sunset in August. The maximum median wind speeds are between 15-20 km/h and occur during daytime.~~ occurs 1 hours before sunset in
March and June and around sunset otherwise. The maximum median up valley wind speeds are between 15-20 km/h. Down

325 ~~at MEE. During the three launches at 08:30, 11:00 and 14:00, a cloud-topped inversion was present around 1500 m (F.a-b) and~~

~~15~~

~~Frequency of T inv. [%]~~
~~Amplitude, T [°C]~~

~~corresponds to the characteristic fog-top altitude during strong Bise wind (https://www.meteoswiss.admin.ch/weather/weather-and-climate-from-a-to-z/fog-top-height.html). The T-profiles reported by the RS present a sharp inversion that is well reported by KENDA-1/MEE. The inversion is placed at the right altitude during the three launches, but the measured gradient of almost 5 °C/80 m is difficult to grasp by the model due to its too-low vertical resolution at these altitudes. The ability to detect these high~~

valley winds are weaker with a median maximum speed of 2-7 km/h reached within the 2 to 3 hours after sunset. ~~Climatology (2013-2022) Campaing 2021-2022 b)~~

~~DEC 25~~
~~a) AUG~~

~~NOV 20~~
~~JUL~~

~~OCT 15~~
~~JUN~~

~~SEP~~
~~10~~

~~MAY AUG~~
~~5~~

~~APR JUL~~
~~0~~

~~JUN~~
~~MAR~~

~~MAY -5~~

~~FEB~~
~~APR -10~~

~~JAN MAR -15~~

~~DEC FEB -20~~

~~JAN~~
~~NOV -25~~

~~0 5 10 15 20 0 5 10 15 20~~
~~Time of the day Time of the day~~

These results
are in good agreement with the 10-year climatology (Fig. S6), which presents however a clear wind speed maximum in July and
an onset of down valley winds 1-2 hours after sunset in spring.

~~Generally, the onset of down valley~~

Similar diurnal and seasonal cycles of the valley wind at the first level are measured by the DWL/MEE at 775 m (Fig. 7.b).
The onset of the up valley winds occurs with the same delay to sunrise (~~Crezee et al. (2022));~~
~~45~~ 4 h) during the summer months but their speed is of

330 ~~altitude inversions may be linked to the fact that the inversion was also present over most of the Swiss Plateau and measured by the RS at Payerne (F.c). The assimilation of RS at PAY probably increases KENDA-1/MEE performance in this case of high atmospheric stability.~~

reduced maximum amplitude (10-15 km/h) than at SMN/MER. At 775 m, the up valley wind intensity is also less regular than
at ground with maximum speed around noon for May to August. The strongest down valley winds are also measured in the
first part of the night, with a higher wind speed (5-10 km/h) ~~than at ground at MER. Additionally, during August, down valley winds occurring 2 hours~~
~~before sunset are measured by the DWL/MEE whereas the onset to down valley winds occuured after sunset at SMN/MER (Fig. 9.a). At 1000 m, the DWL/MEE reports less pronounced diurnal cycles with similar speeds as at 800 m, but the daytime wind~~

compared to the ground at MER. Additionally, during August,
down valley winds occurring two hours before sunset are observed by the DWL/MEE whereas the onset to down valley winds
occurred just after sunset at SMN/MER (Fig. 7.a), a difference linked to the presence of the Brünig Pass (sect. 3.3).

335 ~~The climatology presented in this section provide from the DWL/MEE measurement (reference) and KENDA-1/MEE simulations of wind speeds and directions. Ground~~ Overall, KENDA-1/MEE shows similar results as the DWL/MEE (Fig. ~~10.b). The modeled valley winds evolution are~~
7.d). The modeled valley winds evolution is consistent
with the measurements, including the presence of turbulence leading to daytime varying wind direction. The main differences

~~are a slightly higher up valley wind speed, an underestimation of the down valley winds speed, an earlier onset of up~~

Figure 7. ~~a) Diurnal cycle of the hourly T inversion frequency between ground (590m) and 1000 m. T inversion are accounted when T590m < T1000m. Observations are retrieved from the differences between SMN T MER and FEDRO T BRU, MWR/MEE data are inferred from the difference between the T at the lowest level (590m) of the profile and 1000 m and the same is done for KENDA-1/MEE (705m-1000m).~~
Monthly evolution of along-valley wind speeds [km/h] a) observed at the SMN/MER, b) observed at MWR/MEE, c) modeled at
KENDA-1/MER and d) modeled at KENDA-1/MEE. Sunrise and sunset are represented with dashed lines.

are a slightly higher up valley wind speed, an underestimation of the down valley winds speed and an earlier onset of up valley
winds. The comparison of the first level of KENDA-1/MER (Fig. 7.c) and SMN/MER (Fig. 7.a) indicates an underestimation
of thermally induced along valley wind by KENDA-1/MER, which leads to the absence of diurnal cycle in November and

340 ~~MER, MEE and~~ December. Even in summer months, the along valley wind diurnal cycle is less pronounced in KENDA-1/MER due to the
presence of weak up valley wind in the second part of the night. The modeled data at MER and MEE also present marked
differences, principally a stronger presence of up valley wind during the whole campaign leading to stronger maximum up valley
and weaker down valley wind speeds and the presence of weak up valley wind during all day in winter.

The monthly diurnal cycle of DWL/MEE wind profiles (Fig. 8.a) allows a better visualization of the vertical extent of valley
345 winds. First, the height of the down valley wind determines the limit of the influence of SW synoptic winds. Thermally induced

wind height increases with temperature, reaching ~~only 1000 m in February, 1800 m in May and up to~~

1000 m in February, 1800 m in May and up to 2000-2200 m in July and
August. ~~Second, the onset of up valley wind occurs simultaneous (about 3-4 hours after sunrise) over~~
~~the full valley wind extent,~~ The clear influence of synoptic winds reaches then ~ 1500 m in winter, 2000 m from April to June and 2500 m in July and August. Second, the onset of up valley wind occurs simultaneously over the full valley wind extent 3-4 hours after sunrise,
whereas the onset of down valley wind is delayed from ground to its maximal extent. ~~(Fig. 11.a)~~
~~shows that up valley wind can~~ Up valley wind can then persist until 1-3

~~hr after sunset at the ridge's height. Finally, down valley wind speed decreases~~
~~with altitude and with time after sunset.~~

~~The same representation for KENDA-1/MEE~~ 350 hr after sunset at the ridge's height. Third, down valley wind speed decreases with altitude and with time after sunset. Finally,
the daytime wind direction between 1000 m and 1500 m does not stay constant even during summer months. This might be
related to potential turbulence in valley wind ~~regime~~
regimes (Krishnamurthy et al., 2011), especially when synoptic flows interact with
thermally driven ~~flows or to influence of flows from~~

~~20~~

~~Month~~

~~Month~~

~~Along valley wind speed [km/h] @SMN-MER~~

~~the Sarneraatal. The maximum down valley wind speed also occurs~~ flows, or to influence of flows from the Sarneraatal. In spring and summer, the up valley winds are stronger and
more uniform ~~than at 1000 m and persist longer in the afternoon probably due to the influence of the synoptic winds. At 2000 m, the~~

at 1500 m than at 1000 m and persist longer in the afternoon probably under the influence of the synoptic winds.

355 ~~– Simultaneously with up valley winds, low speed N winds are also measured from May to August between 1300 and 1700~~
~~m and their intensity increases at warmer months.~~

~~16~~

~~– Synoptic winds (ws > 20 km/h in Fig. 8.a)~~ The same representation for KENDA-1/MEE (Fig. 8.b) ~~are very similar to DWL/MEE observations.~~ shows that the vertical extent of the modeled valley wind is comparable
to the observation (± 100 m) ~~expect in April. The main differences are first, an underestimation from ground to~~

~~1600 m of the down valley wind speed until midnight in summer and, second, a too short delay (1-2h) after sunrise of the onset~~
~~of up valley winds between the ground and 1200 m. These statements hold from April to July but not for August. In winter,~~
~~KENDA-1/MEE overestimates the presence of constant down valley winds below 1200 m. However, in November, the modeled~~
~~profiles show continuous up valley winds between 1000 and 1700 m where the DWL/MEE measures mostly down valley winds.~~

except in April, when KENDA-1/MEE modeled a much stronger and higher wind diurnal cycle.
The main differences are, first, an underestimation of the down valley wind speed from ground to 1600 m until midnight
in summer and, second, a 1-2 h too early onset of up valley winds after sunrise between the ground and 1200 m. Third, in

16

November, the modeled profiles show continuous up valley winds between 1000 and 1700 m where the DWL/MEE measures
360 ~~– Higher speeds (ws > 20 km/h) N winds are also present from April to November from the ground to 1000-1500 m. These~~
~~winds originate from Sarneraatal (??) during the late morning and several hours after sunset.~~

~~– The strong influence of foehn in March leads to winds from E direction up to 2500 m, whereas SW winds are prevalent at~~
~~higher altitudes.~~

~~KENDA-1/MEE wind profiles~~ mostly down valley winds. Finally, KENDA-1/MEE overestimates the influence of the synoptic winds leading to the absence of

along valley wind in winter replaced by constant slow down valley winds below 1200 m and to higher up valley wind speed in

spring and summer. The foehn influence in March up to 2500 m is on the contrary well modeled.

Figure 8. Monthly diurnal cycle of the along-valley wind component [km/h] as a function of altitude for a) the DWL/MEE observation and b) the KENDA-1/MEE data. Sunrise and sunset at ground level are given by dotted lines.

3.2.3 ~~Along-valley winds~~

Cross valley winds

The cross-valley winds at MEE can originate from thermally induced slope winds in the Haslital or from valley winds from the
365 ~~1/MEE cell is overlapping the slope towards the Brünig pass so that winds at the junction between Haslital and Sarneraatal can~~

~~influence the mean~~ Sarneraatal passing over the Brünig ~~pass. Slope winds are however more likely to be~~ Pass. Fig. 9.a shows the ~~diurnal and seasonal cycles of the along valley wind speed at SMN/MER during the campaign, whereas the~~
monthly diurnal cycle of the cross-valley wind measured by the

DWL/MEE. During winter, the data are scarce and no particular pattern is visible except the presence of Brünig ~~pass N winds from 800 m to 1500 m in January and February. Cross valley~~

Pass N winds
from 800 m to 1500 m in January and February. During all other months, strong cross valley winds originating from Brünig Pass start between midday and sunset and stop around midnight. They are generally first measured near the ground and reach
1200-1500 m after ~~sunset. Intense~~ sunset, where they reach wind speeds of 20-25 ~~km/h. These N winds~~ km/h and can extend up to 2500 m with weaker speed. These

370 ~~– The main valley wind patterns from March apart are well modeled by KENDA-1/MEE. The main differences concerns the transitions between up and down valley winds. Contrarily to the measurements, the onset of up valley winds during summer months is not simultaneous on the full profile with an earlier onset near the ground. The transition towards down valley wind is also more complex.~~

~~– Frequent N flows from the Brünig Pass are modeled~~ intense north-facing slope winds (> 25 km/h) are also observed between 1400 and 2000 m during some hours around sunset
with a much lower intensity in May. This suggests a circular motion with North updraft winds (median vertical velocity of 1 km/h) that cross the valley at a low altitude, rise against the north facing slope and come back at higher altitude with a South

downdraft component (median vertical velocity of -2 km/h). ~~KENDA-1/MEE also shows cross valley wind patterns (Fig. 13.b) with strong winds from Brünig pass~~ Plots of radial ~~wind speed along and~~ winds perpendicular to the valley ~~(not used in this study)~~ direction clearly present this circulation pattern both in presence of up and down valley winds around sunset (Fig. S9).

375 ~~towards sunset, whereas N flows are~~ KENDA-1/MEE also shows cross valley wind patterns (Fig. 9.b) with strong winds from Brünig Pass from March to August.
These N winds also develop progressively from ground to 1400 m and stop around midnight. They are however modelled earlier than measured, at the time (10:00) of the onset of up valley winds in the ~~Sarneraatal (G). The absence or weakening of up valley winds before sunset in both observations and modeled data (Fig. 10 and 11) are somehow related to these strong cross valley~~

~~500 winds at MEE.~~ Sarneraatal. Winds from the north facing slopes between
1400 and 1800 m are never modeled by KENDA-1/MEE despite their intensity and being systematically ~~measured.~~

~~Figure 13.~~ measured from April to
August. The influence of the Sarneraatal wind on the thermal wind system in the Haslital is not only visible near the ground but

380 also in the difference between the modeled wind profiles at MER and MEE. The along valley diurnal cycle is more pronounced at MER with more constant up valley wind direction at 1000 and 1500 m and higher down valley wind speed, particularly in the morning at 1500 m. KENDA-1 also modeled a lower influence of synoptic winds at MER than at MEE, with almost no at 1500 m even during winter and less influence event at 2500 m in summer. These modeled differences between the two cells can be explained by the different orientation of the valley at both sites and by a already discussed vanishing influence of flows from the Sarneraatal at MER.

Figure 9. ~~a) Monthly evolution of along-valley wind speeds [km/h] at the SMN station in MER during the campaign. Sunrise and sunset are represented with dashed lines. b) 10-year climatology of the monthly evolution of along-valley wind speeds [km/h] at the SMN station in MER. True sunrise and sunset taking shading into account are represented with the dashed-dotted line.~~

~~During the campaign, similar diurnal and seasonal cycles of the valley wind at ground levels are measured by the DWL/MEE at 800 m (Fig. 10). The onset of the up valley winds occurs with the same delay to sunrise during the summer months but their~~

Evolution of the diurnal cycle of the ~~across-valley~~ cross-valley wind component [km/h] as a function of altitude for a) the DWL/MEE measurement

and b) the KENDA-1/MEE. Winds coming from the south-facing slopes take a positive value (red), for the north-facing slope wind speeds values are negative (blue). Sunrise and sunset at ground level are given by dotted lines.

385

~~wind is better defined due to the absence of~~ 18

3.3 ~~Foehn events~~

~~Foehn in~~ Heterogeneity of wind patterns in the Haslital

The design ~~for Payerne, the MeteoSwiss reference measurement station can lead to some bias. (Löhnert et al., 2021) showed that~~ of the Meiringen campaign requires us to compare ~~with the model estimation. Finally, an~~ modeled data to observations at two different sites with different valley directions and different topographic features. The presence of additional wind ground observations in the Haslital and in the Sarneraatal allows a detailed analysis of the effect of the Brünig Pass during clear summer days. The modeled data allow

390 some further insight in the difference of the thermal wind system at MER and MEE in the entire valley volume.
A closer look at the ~~SMN and DWL/MEE wind speeds during a series of clear warm days in July with low cloud amounts (Fig. 12) shows some particularity relative to the previous analysis of monthly median values.~~

~~In MER (Fig. 12.a), a clear diurnal pattern of thermally induced winds is measured. The onset of up valley winds occur~~ SM/MER and DWL/MEE wind speeds during a series of clear warm days in July with low cloud coverage

(Fig. 10) shows some particularities relative to the previous analysis of along valley wind on the basis of a monthly median values. In MER (Fig. 10.a), a clear diurnal pattern of thermally induced winds is measured. The onset of up valley winds occurs at 10:00 and the wind speed strengthens during the day (approximately +4 km/h per hour) to reach a maximum of ~~25 and 30 km/h~~

~~450 at~~ 25-30 km/h at

395 ~~10-year climatology (2013-2022) is presented in Fig. 9.b.~~ 15:00-16:00. The onset of down valley winds occurs at 19:00. During night, down valley winds are constant in direction and drop to 0-5 km/h. It has to be mentioned that the direction of up valley winds at MER gradually shifts from the longitudinal axis of the Haslital towards an enhanced northern component on the 10 and 11 July during the afternoon.

~~In MEE, DWL/MEE measurements are reported at 200 m.a.g.l. Up valley wind is only measured on the 10 July around 08:00 and 12:00 (Fig. 12.a). at 13:00-14:00, the wind direction switches to N and the wind speed increase gradually to reach 40 km/h~~

At the DWL first level (200 m a.g.l.), ~~global radiation, sunshine~~

~~160~~ up valley wind is only measured in DWL/MEE on the 10 July at 13.00-14:00 (Fig. 10.a, color bar). The wind direction switches thereafter to N and the wind speed increase gradually to reach 40 km/h at 20:00. The

400 wind then weakens until midnight and changes direction afterward with a down valley wind direction that persists ~~sometimes~~ occasionally (e.g. on the 12 July) during the morning. Along valley wind patterns following the valley longitudinal axis (W/E) are only observed between 1300 m and 2000 ~~m,~~ m (not shown), namely higher than the Brünig ~~pass altitude. They present then~~ Pass altitude. They then present a standard diurnal cycle with up valley wind measured from 09:00-10:00 to 16:00-17:00 with wind speeds between 15 and 20 km/h.

~~22~~

~~Figure 11. Monthly mean diurnal cycle of the along-valley wind component [km/h] as a function of altitude for a) the DWL/MEE observation and b) the KENDA-1/MEE data. Sunrise and sunset at ground level are given by dotted lines.~~

~~In BRZ, the wind pattern is very different for the 3 selected days (Fig. 12.a).~~ In BRZ, the wind pattern varies during the three selected days (Fig. 10.a). ~~This flows from the Sarneraatal can also explain the time and altitude differences of maximum measured wind speeds with the Rhone valley, even if~~ July 10 and 12, up valley wind begins at 8:00 and
405 ~~speed is of reduced amplitude (10-15 km/h). At 800~~ last until 14:00 with low wind speeds between 5 and 10 km/h. At 14:00, the wind direction switches towards down valley winds

(17-19 km/h), which last until 20:00. ~~Small~~ A small direction change towards WSW ~~occur during the night. July 11, there is no up valley wind phase; the directions remain between NE and E corresponding to down valley wind.~~ occurs during the night. July 11, there is no up valley wind phase with only down valley wind (NE/N). The wind speeds are lower in the morning and strengthen to 20 km/h in the afternoon before to drop at 21:00.

The strong influence of the thermal winds from the Sarneraatal over the Brünig ~~pass is evidenced by this analysis of the wind~~

Pass during hot summer ~~days.~~ days is highlighted
410 ~~direction~~ by this wind analysis at the three stations. An analysis of ground measurements from the BRZ, BRU, LUN, BUC and GIH ~~(G) automatic stations shows that flows measured at the Brünig pass~~ (Fig.

S8) automatic stations shows that flows measured at the Brünig Pass switch towards the Haslital (SSW) 2 to 3 hours earlier
(5:00-6:00) compared ~~to other stations of~~ the onset of up valley wind at other stations in the Sarneraatal (08:00-09:00) and last much longer after sunset, up to 21:00-22:00. ~~The~~
~~low altitude difference between the Brünig pass and the Haslital floor (400 m) explains the wind diurnal cycle measured at low altitude at MEE, that is characterized by N wind from the Sarneraatal during the afternoon, the early evening and also sometimes~~

These winds from the Brünig Pass explain first the N wind observed in MEE during the afternoon,
the early evening and even sometimes in the morning (e.g. on the 11 of July). ~~These winds also strongly influence the diurnal~~ Second, they also strongly influence the diurnal

415 ~~impact of synoptic winds extends to the warmer months except for July and August where down valley winds are still observed. Finally, at 2500 m, just over the mean ridge's height, the impact of synoptic wind is prevailing for all presented months.~~

cycle at BRZ leading to the onset of down valley winds in the early afternoon or even by suppressing ~~the occurrence of~~ up valley winds (July, 11). ~~Their influence at~~
~~MER is however~~ Finally, their influence at MER is weak with only a slight shift of the wind direction towards N in the late afternoon. During these summer days, a standard thermal wind diurnal cycle is ~~then observed in MER and in MEE at altitudes higher than the Brünig pass.~~

~~Concerning the modelled data (Fig. 12.b), KENDA-1/MEE also take into account the influence of the Sarneraatal thermal~~
observed in MER and in MEE at altitudes higher than the Brünig
Pass (not shown).

Concerning the modelled data (Fig. 10.b), the influence of the Sarneraatal thermal winds is well captured by KENDA-1/MEE
420 ~~valley winds. KENDA-1/MEE also overestimates the influence of the synoptic winds leading to the absence of along valley wind in winter, higher up valley wind speed, and, e.g. an earlier onset of down valley wind in August at 2000 m. The foehn influence in March up to 2500 m is well modeled.~~

~~The difference between the modeled (Fig. 10.c) and measured SMN (Fig. 9.a) data at MER indicates an underestimation of thermally induced along valley wind by KENDA-1/MER, which leads to the absence of diurnal cycle in November and~~

so that the differences between MER and MEE are important. At MER, the wind speeds and direction follow a clear thermally

driven valley wind diurnal cycle whereas a relatively stable wind direction from NE during nighttime and NNE during ~~daytime.~~ daytime is modeled at MEE. Speeds at MEE are always equal or higher than over MER with weaker diurnal cycle. The major differences compared to the observations are an overestimated influence of the valley winds from the Sarneraatal leading to no modeled down valley winds at MEE during the night and the morning as well as a shift in wind direction toward N at MER. The differences of

~~the wind speed diurnal cycles at MER and MEE are well modeled by KENDA-1, but the wind speed is almost~~
425 ~~December. Even in summer months, the along valley wind diurnal cycle is less pronounced due to the presence of light up valley wind in the second part of the night. The modeled data at MER and MEE also present marked differences. The along valley diurnal cycle is more pronounced at MER with more constant up valley wind direction at 1000 and 1500 m and higher down valley wind speed, particularly in the morning at 1500 m. KENDA-1 also modeled a lower influence of synoptic winds at MER than at MEE, which is visible at 1500m for cold months and at 2000 m for warm months. These modeled differences between~~

the wind speed diurnal cycles at MER and MEE are well modeled by KENDA-1, but the wind speed is overestimated at both
sites with differences up to +30 km/h.

200

20
150

10
100

0 50

10min/10min 0
Jul 10, 00:00 Jul 10, 12:00 Jul 11, 00:00 Jul 11, 12:00 Jul 12, 00:00 Jul 12, 12:00 Jul 13, 00:00

2022

~~b) 55 350~~
~~MER~~

~~50~~
~~MEE 300~~

~~45~~

~~KENDA MEE~~
~~40~~

~~KENDA MER 250~~

~~35~~

~~200~~
~~30~~

~~25~~
~~150~~

~~20~~

~~15 100~~

~~10~~
~~50~~

~~5~~

~~0~~
~~Jul 10, 00:00 Jul 10, 12:00 Jul 11, 00:00 Jul 11, 12:00 Jul 12, 00:00 Jul 12, 12:00 Jul 13, 00:00~~

~~2022~~

Figure 10. ~~Monthly evolution of the along-valley wind speeds [km/h] for a) the DWL/MEE, b) KENDA-1/MEE and c) KENDA-1/MER. From left to right: along-valley wind speeds at 800, 1000, 1500, 2000 and 2500 m. Sunrise and sunset are represented with dotted lines.~~

a) Measured b) modeled wind speeds (solid lines), wind direction (colored bands and arrow) and sunshine ~~amount for a) the DWL/MEE (800m),~~ duration (orange bars)
for a) the DWL/MEE (800 m), the SMN/BRZ, the SMN/MER and b) KENDA-1/MEE ~~(800m) and KENDA-1/MER (800m).~~

~~3.2.5 Cross valley winds~~

(800 m) and KENDA-1/MER (800 m).

Strong heterogeneities in the wind pattern along the Haslital valley are not only observed in this detailed analysis of thermal wind during summer time but also in the previous analysis of median monthly wind. The comparison of KENDA-1/MER and KENDA-1/MEE (Fig. 6 b and c) wind profiles, confirms the perturbation of the thermal wind diurnal cycle in the Haslital by

430 the ~~two cells can be explained by the different orientation of the valley at both sites and by a reduced influence of flows from the Sarneraatal at MER.~~

~~The mean monthly diurnal cycle as a function of altitude observer over MEE (Fig. 11.a) allows a better visualisation of the vertical extent of valley~~ Sarneraatal winds. In MER, the influence of up valley winds is more pronounced with a clear extension up to 2000 m in

November, March and April, a more delayed onset as a function of altitude in spring and a less turbulent and more constant wind direction during all months (Fig. 7). Generally, the onset of down valley wind is better defined in MER due to the absence of

20

Wind speed [km/h]

Wind direction [°]

winds from the Sarneraatal. It has to be noted that up valley winds modeled at MER take almost the same direction (300-310°) as at MEE (290-300°), even if the valley bends (≈ 30°) between the two sites, except in the early morning (sunrise to 10:00)

~~when up valley winds come from W at low altitude (from MEE direction). This near~~

435 when up valley winds come from W at low altitude (from MEE direction). This near ground direction difference is similar to the observed winds at MEE, but happens earlier (from sunrise) and disappears at 10:00. Modelled down valley winds in MER always follow the main longitudinal valley axis, like in MEE.

3.4 Foehn events

Foehn is a katabatic wind bringing ~~generally~~ strong warm and dry ~~downdraughts associated generally with clear weather (foehn window). The following case study~~ downdraught usually leading to clear weather conditions. The study
440 of the T during foehn events combines all the periods where foehn was measured at the SMN station in MER, ~~25~~

according to

the foehn index. The ~~selected data represent~~ study on the wind is however performed on only three selected events (10-16 March 2022/19-22 March
2022/26-24 April 2022) representing 117 hours ~~mainly occurring in March.~~ of foehn during clear weather in March, while the April and June episodes
presented a slightly overcast sky (50-70% of maximum global radiation).

~~3.3.1 Temperature~~

~~14.a shows that the MWR/MEE tends to measure lower T than the SMN/MER. However, the 0.5 to 1.5°C differences can be~~
3.4.1 Temperature during foehn events

445 ~~3.2.4 In-depth analysis of selected clear summer days~~

During foehn events, the MWR/MEE tends to measure 0.5-1.5°C lower T than the SMN/MER (Fig. 11.a), which can be partially explained by the different sites locations and altitudes. In contrast, a significant ~~T underestimation (-2 to -4 °C) by KENDA-1 is observed during foehn events, without the mean diurnal~~
~~cycle measured during the whole campaign (Fig. 5).~~ KENDA-1/MER and KENDA-1/MEE
T underestimation of -2 to -4 °C is observed regardless of time of day. Furthermore, the differences categorized according to ~~wind speed (Fig.~~
~~14.b)~~ measured wind speed (Fig. 11.b) ~~shows that the vertical extent of the modeled valley wind is~~
show that larger wind speeds (> 20 km/h) induce larger median T underestimations. Saigger and Gohm (2022) performed simulations in the Inn valley with the Weather Research and Forecasting model and observed

~~similar bias at low altitudes during~~

450 similar bias at low altitudes during an intensive foehn event. Additionally, Tian et al. (2022) also report significant cold and moist biases in the model during foehn hours. Note that the KENDA-1/MER is in better agreement than KENDA-1/MEE with SMN/MER (not shown), which can indicate significant differences in the foehn influence at the two stations.

~~Figure 14. Box plots and whiskers of ground T differences between the SMN/MER station and the MWR/MEE (blue), the SMN/MER station and KENDA-1/MEE (red), the SMN/MER station and KENDA-1/MER (pink) as a function of a) the hour of the day and b) the 10 m measured wind speed at SMN/MER. The dashed lines represent the median of the different distributions.~~

The comparison of T profiles during foehn events in March (Figs. ~~??).~~ S11 and S12) shows that KENDA-1/MEE and KENDA-1/MER underestimates the T not only at the surface but up to 900-1400 m depending on the event. In some cases, KENDA-1

~~missed the T increase due~~

455 ~~at 20:00. The~~ missed the T increase due to foehn but in other cases, KENDA-1 follows the T evolution but with a smaller T gradient. The median T bias of 2-4°C ~~is similar~~

~~along the profile (mettre reference fig ap 26) and at the surface and is reinforced when a T inversion missed by KENDA-1~~
observed at the surface is also measured along the profile and is reinforced when a T inversion missed
by KENDA-1/MEE precedes the foehn event. The T increase due to the foehn breakthrough measured by the MWR/MEE is
delayed by less than one hour compared to the SMN/MER detection. Similar time delays of about one hour are modelled by
KENDA-1, with shorter delay at MER than at MEE as expected by the orientation of the Haslital and the provenance of foehn.

460 ~~and~~ 3.4.2 Wind

DWL/MEE measurements (Fig. 12.a) shows the extend of the higher wind speeds induced by the foehn from ground to the
ridge's height (1800-2000 ~~m).~~ m) for a selection of three cases in March and April 2022. The foehn breakthroughs are nearly
simultaneous at ground (SMN/MER) and up to 1000-1500 m at ~~MWR/MEE~~ DWL/MEE for the events of March 11 and April 23. ~~However, an~~
~~important delay of ≈ 3 hr is measured between 800 and~~
~~1300 m for March 20. Foehn winds are however measured from 1300 m up to the ridge at the same time as at the SMN/MER~~

For March

Figure 11. Box plots and whiskers of ground T differences between MWR/MEE and SMN/MER (blue), KENDA-1/MEE and SMN/MER
(red) and SMN/MER and KENDA-1/MER (pink) as a function of a) the hour of the day and b) the 10 m measured wind speed at SMN/MER
for all foehn events during the campaign. The dashed lines represent the median of the different distributions and n is the number of cases in
each of the categories.

20, an important delay of ≈ 3 hr is measured between 800 and 1300 m, whereas foehn winds are measured from 1300 m up to
465 ~~at the three stations~~ the ridge at the same time as at SMN/MER. The maximal measured wind speeds at 800 m in DWL/MEE (60-75 km/h) are

higher than at the SMN/MER (45 km/h), especially for the event of March 11.
During the first selected episodes (11.03) the foehn arrival is modeled 2 hr too early by KENDA-1/MEE (Fig. ~~15.b)~~ 12.b) with

strong winds (60 km/h) from SE between 800 and ~~1000m. At 11:00, the measured foehn arrival, the KENDA-/MEE wind~~
~~direction is coherent with measurements but speeds are overestimated between ground to ridges with differences up to~~ 1000 m. After the foehn
breakthrough (11:00), the KENDA-1/MEE wind
direction is coherent with measurements but wind speeds are first overestimated by 15-30 km/h between ground to ridges height

470 during 4 hr (Fig. S13), then underestimated during 2 hr before being in accordance with measurements for the rest of the event.
For KENDA-1/MER (Fig. ~~15.c), the same delay in the foehn breakthrough is observed. It happens over a larger extent (800 to 1200~~
~~m) with even higher wind speeds (> 100 km/h). This overestimation is constant during the entire event.~~

~~For March 20,~~ 12.c), the same premature onset in the foehn breakthrough is observed but over a larger vertical extent
(800 to 1200 m) and with even higher wind speeds (> 100 km/h) lasting during the entire event.

During the second episode, KENDA-1/MEE models correctly the 3h delay between SMN/MER and DWL/MEE measurement
~~is modelled by KENDA-1 (Fig. 15.b and Fig.~~
(Fig. 12.b) but extends it up the ridge height contrarily to the measurements. The KENDA-1/MEE wind speeds tend to be

475 ~~winds so that the differences between the two analyzed sites (MER/MEE) are important. At MER, the wind speeds and direction~~

overestimated (+15 km/h) from ground to ~~1100m during the entire event. From 1100 m to the ridge's height the wind is underestimated~~ 1100 m
during the entire event and underestimated from 1100 m to the ridge's height

(-30 km/h) ~~during~~
~~the first 5 hours.~~ the first hours following the breakthrough. KENDA-1/MER modelled again wind speeds up to 100 km/h with a
foehn breakthrough at the same time as the SMN/MER (Fig. 12.c). At the very end of the event (March 20 at 23:00), ~~KENDA-1 keeps~~ KENDA-
1/MEE and KENDA-1/MER keep showing ~~strong foehn winds between 900~~
~~and 1500 m while nothing is measured by SMN/MER and DWL/MEE. At MER, KENDA-1/MER modelled again wind speeds~~
~~up to 100 km/h with a foehn breakthrough at the same time as the SMN/MER.~~

foehn winds between 900 and 1500 m while no wind is measured (SMN/MER and
DWL/MEE).

480 ~~the observations (Fig. 12.b and (H Fig. H1.a) are a too strong influence of the valley winds from the Sarneraatal leading to no~~
~~modeled down valley winds at MEE during the night and the morning as well as a wind direction shifted~~ Few DWL/MEE measurements are
observed during the third selected episode, but the timing of the foehn breakthrough and
the wind speed are similar at SMN/MER and DWL/MEE. The breakthrough is modeled with a long delay by KENDA-1/MEE

but almost in time by KENDA-1/MER and the end of the foehn episode is also delayed by both KENDA-1/MEE and KENDA-1/MER. The wind speed is also overestimated if compared to SMN/MER, particularly by KENDA-1/MER with maximum speed higher than 75 km/h during the whole event.

~~The cross-valley winds at MEE can originate from thermally induced slope winds in the Haslital or from valley winds from the~~ To summarize, the ~~modeled data show a better representation of the temporal extent of the foehn events over MER than over MEE. Despite the good temporal representation of foehn arrival, the speed up to 110 km/h from ground level to 1500 m is twice as big as what is measured at MEE, 5 km further~~ three analyzed events exhibit some similarities but also large differences. ~~Literature (Jansing et al., 2022) cites three main foehn types~~

The foehn breakthrough is often observed some hours later by DWL/MEE than by SMN/MER and not always simultaneously in the entire profile. The wind speed at the DWL/MEE first level is usually similar to the one at SMN/MER. KENDA-1 tends to model the foehn arrival and end with positive or negative time shifts at both stations. The most critical point ~~located approximately in the middle of the valley floor, SW to the pass 1. The model cell only gives an averaged value of~~ concerns the very high KENDA-1/MER modeled speed up to 110 km/h from ground level to 1500 m that is twice faster than the DWL/MEE observation, 5 km further

~~winds originating from Brünig pass are measured up to 1500 m during all other months with a wind speed~~ down in the valley. Even though the Haslital is narrower just before MER, such wind speeds difference is subject to a discussion about a potential large overestimation of the winds at this location. ~~The~~ Finally, the simultaneous wind speed overestimation and the T underestimation by KENDA-1 during foehn events are difficult to explain since a stronger foehn should allow for a greater T increase.

~~A moist bias of the model is a hypothesis for the observed~~

~~follow a clear thermally related valley wind cycle with an onset of the up valley wind from 09:00 apart, a maximum wind speed of 30-35 km/h around 14:00 and an onset of down valley wind at 18:00 with decreasing wind speeds (3-5 km/h) until the next morning. At MEE the modeled winds show~~ Figure 12. Wind speed profiles [km/h] time series from a) DWL/MEE, b) KENDA-1/MEE and c) KENDA-1/MER during a selection of 3 foehn events: left 11-12.03.2022, middle 19-22.03.2022 and right 23-24.04.2022. Wind speeds [km/h] from the SMN/MER are given in the lower part of each figure. The solid line represents the foehn breakthrough.

~~Wind speed [km/h]~~
~~Wind speed [km/h]~~

~~Wind direction [°]~~
~~Wind direction [°]~~

4 Discussion

~~higher altitude with a South~~ Complex topography, landscape heterogeneity and specific thermal wind regimes challenge the models' spatial and temporal resolutions, their performance in data assimilation and the parameterization of multi-scale processes. The discussion will consequently focus on three points, the specificity ~~and modeling challenges~~

~~1.1.1 Near-surface Temperature inversion~~

of the terrain around the campaign site, the comparison of the observed wind and T profiles with previous observations in the Alps and the model performances in Meiringen.

~~The two used cells are highlighted in yellow.~~

4.1 Topographical and methodological challenges

~~The difficulty to model the physical phenomena taking place in complex topography comes first from~~ The Haslital presents several peculiar topographical and landscape characteristics, particularly in the vicinity of the ~~lake (< 100 m) can also cause this difference at the BRZ station due to its higher thermal inertia.~~

~~49~~

~~Figure I11. Wind speed profiles comparison [km/h] timeseries between KENDA-1/MEE and DWL/MEE during a selection of 10 clear days middle of July (July 15th is overcast). Sunshine and sunset are represented by the dashed line.~~

~~955 Appendix II: Valley winds during clear days~~

~~50~~

~~Figure I1. T profiles [°C] timeserie from a) MWR b) KENDA-1 MEE and c) KENDA-1 MER. during a selection of 3 foehn events during the campaign: left 11-12.03.2022, middle 19-22.03.2022 and right 23.04.2022. T, wind speed [km/h] and direction [°] from the SMN MER are given in the lower part of each figure. The solid line represent the begining of the foehn event.~~

~~Appendix I: T comparison during foehn~~

~~The effect of foehn on T is variable: during March 20, the foehn event started at 23:00 and inhibited the formation of the T inversion by destroying the stable layer built so far. This induced mild T during the night compared to previous days (I, Fig. I1.a). On~~ campaign
site (Fig. 1). Its junction with the ~~Sarneraatal, 4 km downstream, via the Brünigpass~~ Sarneraatal via the Brünig Pass links the two valleys with an angle of ~~≈~~ ~ 90°, 400 m above the
valley floor. ~~Considering this small altitude difference, this pass can even be considered as a tributary inlet. It allows the winds from the Sarneraatal to easily reach the Haslital with a cross-valley wind component,~~

It allows winds from the Sarneraatal to easily reach the Haslital with a cross-valley wind component similar to
down slope winds and to disturb its along valley wind ~~system (Fig. 10). The location of MEE just under the Brünig pass~~ system. The location of MEE just under the Brünig Pass has to be taken
into account for comparison between MEE and MER results. Based on numerical simulation in the Alpine Inn Valley, Zängl

505 (2004) suggests that variations in wind intensity are mainly related to tributary valleys, which increase or decrease the mass flux in the main valley. ~~As such low pass~~ In this regard, low passes can have similar effects as tributaries. Moreover, the model cell over MEE overlaps the ~~slopes towards the Brünigpass while the observations over MEE are characterized by a single~~ slope towards the Brünig Pass, so that KENDA-1/MEE reports an overlay of winds from the Brünig Pass and in the Haslital. DWL/MEE, on the other hand, ~~for the event of March 11 and April 23, the foehn events start around 11:00, and the T increase is not as~~

~~51~~

~~Figure I2. T profiles comparison [°C] between KENDA-1/MEE and MWR/MEE during a selection of 3 foehn events during the campaign: left 11-12.03.2022, middle 19-22.03.2022 and right 23-24.04.2022. Wind speed [km/h] and direction [°] from the SMN MER are given in the lower part of each figure. The solid line represent the begining of the foehn event.~~

~~960 important. For March 11, the foehn breakthrough happens at 11:00 with a T increase of 8 °C between 08:00 and 09:00 and a second T increase of 3 °C between 11:00 and 12:00. The MWR measures the same T evolution. With a delay of less than an hour, KENDA at MEE and MER (Fig. I1.b-c) show the same temporal T evolution as at SMN. However, the temporal T gradients are smaller because of the missed inversion of the previous night and the underestimated T during the foehn event. The two modeled T evolution exhibits a delay of one hour. KENDA-1/MER T increase happens before that from MEE which~~

~~965 is coherent with the orientation of the Haslital and the provenance of foehn. For the rest of the profile, the rapid T increase is observed between the ground and 1200 m and nearly constant T are measured in that part of the profile. KENDA-1 shows the same pattern with a negative T bias of 2 °C that grows up to 4°C when maximal wind speed is reached. For March 20, at ground, the foehn breakthrough at 11:00 breaks the inversion around midnight and maintains mild T until the arrival of the sun where the T further rise according to a classical daily cycle. KENDA-1 ground T at MER and MEE does not show any T increase during~~

~~970 the night and therefore underestimates the T. During daytime, the T underestimation is the same as for days without foehn. For the rest of the profile, the T are better modeled than for the 11.03. The T underestimation (2-3 °C) again extends from ground to 1200 m but this time it remains only in the first 4 hr of the event. Afterward, this underestimation is constrained under 900 m. Finally for the 24th of April, at ground, MWR and SMN T are the same until the foehn breakthrough at 11:00. The two measurements then show a 2 °C difference during the foehn event~~ only observes winds in the middle of the Haslital. Consequently, the differences between the
modeled T/wind ~~within it, which will induce bias when compared with high horizontal resolution measurements. Consequently, differences between the model and the measurements cannot only be categorized as model errors.~~

averaged values and the observations cannot be only considered as model errors only.

510 ~~explained by the small size of the data set as well as the different locations and altitudes between both T measurements.~~ Additionally, the curving of the valley between MER and MEE implies that the same valley side faces different ~~orienta-~~
~~tions along the Haslital and consequently different heating time by the incoming solar radiation of the system (Fig. 1), slope at~~

orientations
along the Haslital leading to different heating by the incoming solar radiation. The presence of large lakes covering the entire
valley floor in its lower part, 5 km ~~after~~ down valley of MEE, modifies the heat exchange between the surface and the atmosphere due
to their high thermal inertia. ~~The presence of lakes can influence the T profiles along the valley, and consequently the pressure difference, as well as~~ Their influence on the T along the valley can affect the pressure difference, and consequently the
time, extent and strength of the thermally induced valley winds. When comparing observed phenomena with similar studies,

515 ~~an intensive foehn event. Additionally, Tian et al. (2022) also report significant cold and moist biases are found~~ the combination of the above mentioned peculiar features gives explanatory hints for the observed differences. Finally, this
study is based on monthly median values, so that the averaging artifacts have to be considered, e.g. for the analysis of maximum
wind speed, the onset time of valley wind or wind directions. In that sense, this analysis focused on climatology and not on the
forecast skills of COSMO-1E.

4.2 Comparison of observed phenomena with other studies

520 ~~to foehn but in other cases, KENDA-1 follows the T evolution but with a smaller T gradient. The mean~~ 4.2.1 ~~T inversion~~

Occurrence of surface based T inversion in valleys

T patterns in MER follow a classical diurnal and seasonal cycle. The most important feature in the context of this study is the
presence of frequent ground T inversion (Fig. 2.a, 5.a). According to a 3 years study in the French Jura performed over 16
station pairs ~~(Joly and Richard (2019)),~~ at different altitudes (Joly and Richard, 2019), T-inversions are equally common in winter and summer (60% of the
time), but with a larger amplitude (3°C) in winter than in summer (2°C). Additionally, ~~a study conducted by Rupp (2020) examined 13 years of hourly air temperature data~~ temperature inversion occurred also more

25

525 ~~3.3.2 Wind~~

~~DWL/MEE measurements (Fig. 15.a) shows the extend of the higher wind speeds induced by the foehn from ground to the mean~~
than 50% of the time in a 13 years T climatology in the Cascade Range, USA, at comparable ~~altitudes. The findings reveal that temperature inversions~~
~~occurred more than 50% of the time,~~ altitudes (Rupp et al., 2020), with
the formation and dissipation of inversions consistently ~~lagging behind local sunset~~

~~600 and sunrise times by approximately four hours.~~ having an approximately four hours time difference from sunset and
sunrise. Finally, a 56-year climatology in the Austrian Alps (Hiebl and Schöner, 2018), shows that T inversions occur throughout
the year with a frequency of about ~~30%,~~ 30% from October to January and 15% from April to August. ~~Their~~ The intensity, magnitude and
thickness ~~follow a similar seasonal pattern as observed in the Haslital. Inversions are~~
~~more frequent in eastern Austria and less frequent in the large~~ of these surface T inversions follow a similar seasonal pattern as observed in the Haslital. Inversions are more frequent

530 ~~station. The maximal measured wind speeds at 800 m in MEE~~ in eastern Austria and less frequent in the wide western valleys and ~~basin of Austria~~ basins and almost vanishing in high-Alpine summit area.
This ~~study in the Haslital show similar near ground T inversion occurrence (7.a). During the campaign~~

campaign (Nov-Aug) in the Haslital (Fig. 5.a) shows a similar occurrence of near ground T inversions, i.e. 30% between
the two ground stations (MER-BRU) and ~~for 40% of the time in~~
~~the MWR profile.~~ 40% in the MWR profiles. Amplitudes are similar to the results from Joly and Richard
(2019) with slightly higher ~~number during winter~~
~~month~~ values during winter months (+ 1°C). The seasonality of the phenomena is mainly characterized by
the frequency of T ~~inversion~~ inversions along the day in winter and the onset of the erosion process. Similar ~~number than (Hiebl and Schöner, 2018) are found concerning the evolution~~
~~of the phenomena throughout the months:~~ seasonality as in Austria

535 ~~km/h (J, Fig J1). This overestimation lasts for the first 4 hr and then turns out to a KENDA-1/MEE underestimation of wind~~
~~speed. This happens for 2 hr and then finally KENDA-1/MEE is~~ (Hiebl and Schöner, 2018) are found with 14.3% of T inversions from April to August and 46% from November to February.

4.2.2 ~~Valley winds~~

Characteristics of valley winds in the Alps

Previous ~~works have been done on diurnal valley winds in alpine valleys. The result obtained are compared with studies performed~~ studies on diurnal valley winds in alpine valleys took place in the Rhone (Length = ~~140km,~~ 140 km, Floor Width = ~~4-5km, Ridge to Ridge Width = 15km,~~ 4-5 km,
Ridge to Ridge Width = 15 km, Schmid et al. (2020)), in the Adige (L = 140 km, BW = 2-3 ~~hours around sunset. At 1500 m the effect of synoptic winds~~ km, RRW = 8 km, Giovannini
et al. (2017)) and in the Inn valleys (L = ~~140km, BW = 4-5km, RRW = 20km,~~
140 km, BW = 4-5 km, RRW = 20 km, Adler et al. (2021)). ~~The valleys of these 3 studies are relatively long and wide compared to the Haslital (L = 30km, BW = 1.5km,~~
~~RRW = 5km, Fig. B2),~~ These three valleys are

540 ~~15.c) but, contrarily to DWL/MEE, up the ridge height. The KENDA-1/MER~~ relatively long and wide compared to the Haslital (L = 30 km, BW = 1.5 km, RRW = 5 km), which can induce differences in the
thermal valley wind systems. All three studies make a selection of valley wind days by using threshold on minimum global solar radiation or up valley wind speeds and selected global weather type.

Similarly to the observations in the Haslital, the wind direction change in the Rhone valley (Schmid et al., 2020) occurs for altitudes up to about 2 km a.g.l. with diurnal pattern undergoing significant changes during the course of the year. During

545 summer, maximum up valley speeds of 30-35 km/h are found above the Rhone valley during the early afternoon at 200 m a.g.l. Similar timing for maximum up valley winds are found at both MER and MEE, but with reduced speeds both at ground (SMN/MER, 20-30 km/h) and at 200-300 m a.g.l. ~~over MEE (15-20 km/h). The applied monthly median,~~

~~625 without selection of days favorable to thermal valley winds, can also explain the lower maximal up valley wind speed in the Haslital, but other causes bounded to the valley size and to further topography features cannot be excluded. At MEE, in fact, the highest wind speeds of 30 to 45 km/h are found~~ (DWL/MEE, 15-20 km/h) that relates to some extend to the absence of clear-sky days selection in this study. At MEE, the highest wind speeds of 30 to 45 km/h are found however later on, at 18:00 and 19:00, between 800 and 1400 ~~m. They correspond to valley winds from the Sarneraatal with a direction of 50° and contribute to the main down valley wind component. They are also observed at the same time at LUN and BRU (Fig. 13 and G1) and are strong enough to flow into the Haslital. The N-S~~

m and correspond to valley winds from the Sarneraatal. The topographic difference between

550 ~~related to distinctively different synoptic situations for Switzerland. During the most typical deep foehn situation occurring 90%~~

the Brünig Pass and the standard tributaries' inlet ~~of tributaries are also present near the campaign site at Sion. Due to the low altitude of the Brünigpass, the Sarneraatal can be considered as a tributaries, but with effect at higher altitude. Concerning down valley wind~~

at the campaign site in Sion ~~and on the interaction of along and cross valley flows.~~ can also explain the time and altitude differences
of the strongest winds. Concerning down valley wind speeds, Schmid et al. (2020) report their presence between 500 and 1000 m.a.g.l with a speed of about 15-20 km/h. They occur in the second part of the night in spring and summer, and during the entire night in winter. Several differences are observed in the Haslital: 1) down valley winds reach ground even in summer (Fig. ~~9)~~ 7) and extend up to 800-1000 m.a.g.l., 2) their speed gradually decrease around the night with almost no wind between 00:00 and the

555 ~~differences.~~

new onset of up valley winds for all the studied period and 3) at MEE, maximum down valley wind speeds are measured from March to July at the same altitude as in the Rhone valley but with lower wind speeds (10-15 km/h). If the last difference can also be explained by the applied monthly average, the timing and extent of the down valley winds probably relates to topography differences.

~~The work of Giovannini et al. (2017) in the Adige valley in the Italian Alps~~ 26

~~The comparison of T profiles during foehn events (I, Fig. I1.a) shows that KENDA-1 at both MEE and MER~~ In the Adige valley in the Italian Alps, a campaign in May-August ~~shows similar results as found in the present study. The wind speed measured at ground show maximum up valley wind speeds between 15:00 and 16:00 being~~

(Giovannini et al., 2017) observed maximum up valley
560 ~~and energy exchanges. Additionally, in regions with complex topography, the terrain affects the distribution and exchange of energy between air masses. Finally, the Haslital has several peculiar topographical characteristics along its path and particularly near the campaign site~~ wind speeds between 15:00 and 16:00 that are stronger near the valley outlet (20-30 km/h) and gradually weaken (8-10 km/h)

towards the highest valley parts situated 100 km further up. Surface down valley wind speed appears to be very weak, between 0 and 5 km/h, and nearly constant in the entire valley. However, ~~their mean onset is delayed to 00:00 which is not the case both in the Haslital, for the entire climatology (Fig. 9) or for selected valley wind days (Fig. I1.a), and in the Rhone valley. Wind profiler data from the outlet of the Adige valley show that the strongest up valley winds are recorded between 1000 and 1400 m.a.g.l. at 18:00. Similar late, maximal~~

650 up valley wind speeds are also recorded at MEE (Fig.11.a) if Brünigpass winds are accounted for up valley winds (Fig. 13). Contrarily to both Schmid et al. (2020) and this study, the down valley winds of the Adige valley gradually weaken towards higher altitudes at 00:00 and 02:00. For the rest of the night, stronger wind are also found between 500 and 1000 m.a.g contrarily to the Haslital and the Rhone valley, the down valley
wind onset is delayed to 00:00. Wind profiler data from the outlet of the Adige valley show that the strongest up valley winds are recorded in the late afternoon, similarly to the observations at MEE (Fig.8.a). Contrarily to both, Schmid et al. (2020) and this

565 similarly study, the down valley winds of the Adige valley gradually weaken towards higher altitudes around midnight. For the rest of the night, stronger wind are also found between 500 and 1000 m.a.g.l. similarly to the observation in the Rhone valley (Schmid et al., 2020).

Finally, concerning the onset of up valley wind, both the time and the pattern of the transition are similar in the Rhone, the Adige and the Haslital valleys. The onset occurs 3-4 hours after sunrise with flows that move almost simultaneously

valley. The onset occurs 3-4 hours after sunrise with flows that move almost simultaneously between 0

570 The difference between the location of the observations and the extension of the model cell over MEE needs to be taken into account. Indeed, a part of this cell to 1500 m.a.g.l from June onwards. The morning transition occurs at the same time at all heights while the up-valley wind starts weakening from the bottom while, during the evening
transition, the wind direction down wind begins at ground due to progressive cooling of the lowest atmospheric layer (Zängl, 2004) and thickens during the night. Note that, Schmid et al. (2020) reported a delayed onset as a function of altitude in autumn but unfortunately, no data were acquired in the Haslital
during this period.

during this period in the Haslital.

The CROSSINN campaign (Adler et al. (2021)) was performed from August to October in the lower part of the Inn valley al., 2021) was performed from August to October in the lower part of the Inn valley
575 For instance, KENDA-1 cell lies on the pass area implies that wind originating from there are completely comprised in the cell while along valley wind from the Haslital bottom part are only partially comprised in it.

Additionally, the change in orientation and focused on cross valley winds. During two days of September, the wind field in the vertical plane across the valley show

subsidence around 13:30 and 14:30 without any particular cross valley wind direction above the valley floor center. In the second part of the afternoon (15:00-17:00), the valley atmosphere presents an enhanced cross valley wind circulation. Over the south facing slope of the valley, subsidence prevails, while over the north facing slope upward motion is measured. This flow pattern form a closed circulation cell with a clear cross-valley component with comprising a northerly component in the lower 700 m.a.g.l.

580 MER being more orientated towards E than at MEE. and a southerly component above. Similarly to the Inn valley, the Haslital at MEE also lies in the E-W direction (slope however

direction. A cross-valley
circulation is also observed from March to August (Fig. 9.a), with a wind direction change from N to S between 450 and 850 m a.g.l and a stronger pattern in Summer. In the Haslital, the separation between north and south facing wind lays between 700 and 1000 m.a.g.l. The particularity in
MEE is that the lower part of the cycle (winds from the south facing slope) is probably mainly due to valley winds from the Sarneraatal. However the upper part of the cycle is a good clue that this type of circulation occurs in the Haslital However, in MEE, valley winds from the Sarneraatal are probably the main drivers of
this circulation cell at sunset.

4.3 Model performance

585 Finally, most of the data representation are using the monthly median value of hourly data. No filtering of data relative to particular weather type (except for precipitation periods) is done. It allows to get ride of special meteorological cases in a climatological way but does not allow to evaluate particular cases. The effect of averaging has to be taken into account for the analysis of maximum valley wind speed or onset of valley wind. This is especially the case for wind directions: the aggregation

590 can lead to angles that are never observed. Therefore, this study does not allow to make prediction of model performance for forecasting.

According to the presented monthly median values, KENDA-1 is generally able to capture the main features of the observed atmospheric conditions and the differences to the observations are comparable to those obtained from REM instruments. T profiles climatologies mostly show T difference <1 °C. Moreover directions and speeds of
the diurnal valley winds are in agreement with the measurements. found in standard MeteoSwiss seasonal

verification with radiosonde and surface observations averaged over the whole model domain. This is remarkable given the complex topography in the region of this study. However, some meteorological phenomena specific to mountainous regions and/or particular synoptic conditions are hard to capture by the model and thus can lead to larger differences between model and

590 observations.

~~Figure 15.~~ 4.3.1 ~~Temperature~~

~~The analysis of the daily cycle, averaged over the entire campaign~~ KENDA-1 skills in temperature estimate

The analysis of the daily cycle shows that the majority of ground T differences with respect to observations lays between ±−3 °C (Fig. ~~5) with a nighttime overestimation and a daytime~~

~~underestimation by KENDA-1. Two one-year analysis over the COSMO-2 (Voudouri et al., 2018) and COSMO-1E (Voudouri et al., 2021) domains~~ 4) with a nighttime overestimation and a daytime underestimation by KENDA-1. In a study over complex topography (Alpine Arc and particularly Switzerland and northern Italy) ~~find a similar daily cycle in ground T mean error, but of reduced amplitude. COSMO-2 show a ~0.8 °C bias during daytime and unbiased T during night while COSMO-1E has a ~0.5~~ Voudouri et al. (2021) found a similar daily cycle in ground T mean

595 ~~presence of frequent ground T inversion (Fig. 3.a, 7.a).~~ error in COSMO-1E forecasts, but of reduced amplitude (-0.5 °C bias during day and a +0.5 °C bias during ~~night. An additional study (not shown) performed on COSMO-2 (v.5.03)~~

night). Despite the complex topography around MER and the induced elevation bias, the modeled climatology of ground T is comparable to standard verification results, even if differences up to 8° C are ~~found. The main explained source of ground T differences is caused by missed surface T inversion. The frequency of this phenomenon is partially missed by KENDA-1 from March to August (7.a) and its amplitude is underestimated for all month under study. It is especially the case at the end of March, when sharp inversions form due to enhanced night time radiative cooling and important global solar~~

found in some periods. The main explained source of ground T differences is caused by missed surface T inversion. The frequency of this phenomenon is partially missed by KENDA-1 from March to August (Fig. 5.a) and its amplitude is underestimated for all months. This is especially the case at the end of

600 March, when enhanced night time radiative cooling and important global solar radiation form strong inversions. The observed amplitude difference are mainly due to an underestimation of T at ground (Fig. 4). A work carried by Sekula et al. (2019) on the nonhydrostatic model CY40T1 AROME CMC (2km horizontal resolution) showed the same general overestimation of the minimum T in valleys bottom. The largest differences were measured during strong high-pressure systems which favors cold air pools formation leading to ~~e.g. T overestimations of up + 7 to 9 °C during 10 days in March.~~

T overestimations of up + 7 to 9°C during 10 days in March.

605 ~~(Nov-Aug), T inversions were present 30% of the time between the two ground station~~ A preliminary analysis on KENDA-1 behaviour during this strong T inversions ~~(not shown) show that the observed differences~~ show that the observed differences are probably due to a too low model first guess ensemble spread. The model is too much trusted in the model-observation weighting scheme and measured T at MER are therefore not used in the model assimilation step. Another hypothesis is that a too large observation error is assigned to the station of MER (1.17K end of March). Additionally, at this period, the ~~model predictive capacity concerning ground relative humidity is variable. During day, the observation and KENDA-1 data~~ difference between observed and modeled ground relative humidity (RH) ~~interval during day (not shown) but at night the model is heavily~~ are within ± 5% during day but, during night, the model is heavily

610 drier (-20 to -30 % ~~RH). According to~~

~~700~~ RH, not shown). According to Westerhuis et al. (2021), artifacts from the NWP ~~are to~~ can be expected under conditions favourable to surface T-inversion. The COSMO-1E vertical coordinates follow the terrain. Therefore, ~~over complex topography, T-inversions and the surface of the vertical grid used by the model intersects which can produce numerical artifacts. The systematic T underestimation during night can also be driven by errors of the model cloudiness. An overestimated model~~ in complex topography, numerical artifacts may originate from the intersection between T-inversions and the surface of the vertical grid used by the model. The systematic T underestimation during night can also be driven by an overestimated modeled cloudiness ~~could prevent the model surface to cool down due to too low~~ involving underestimated out-going long-wave radiation. Further ~~investigation have to be done using either the ceilometer or~~

~~705 the DWL to estimate the cloud cover over the Haslital valley and~~ investigations ~~are~~

~~70 needed.~~
have to be performed using ceilometer and/or

615 ~~(L = 140km, BW = 2-3km, RRW = 8km,~~ DWL observations to estimate the model skill with respect to cloud cover. Finally, the differences with observations can also
originate from a modeled ongoing turbulent mixing ~~in the model can be present while~~ whereas in reality a cold pool ~~might be formed and~~ with a full or partial decoupling from the
~~flow above could also cause the observed differences with observations.~~

above flow is present in the valley.

For profile comparison, MWR T is ~~considered~~ taken as the reference, but ~~the MWR T~~ its reliability, especially at ~~higher altitude, has to be taken into account~~ high altitude, has to be considered in
the evaluation of KENDA-1 results. Löhnert and Maier (2012) performed a MWR-RS comparison and showed that random error

620 inherent to the measurement principle can be important in some cases. ~~Random~~ They showed that random errors range grows up to 1.7 K at 4 km height, due to a 95% influence from the used apriori profile. KENDA-1 and MWR T profiles differences are constrained to ± 1 °C for all altitudes between 1400 and 2200 m both day and night except in June and July (Fig. ~~6). Differences up to -3 °C can occur near the ground in winter or at ridge level in July. This~~ 2.b). Differences up to
-3 °C can occur near the ground in winter or at ridge level in July. The near overall negative bias can ~~be explained by several way. First,~~ mainly be explained by
two factors: first, the MWR is susceptible of errors especially for higher altitudes with RMSE between 1 and 1.5 °C (Liu et al.,

~~of the time, the foehn flow is accompanied by a deep layer of southerly or southwesterly winds. The 3 selected cases can be characterized as deep valley foehn.~~

~~The simultaneous wind speed overestimation and the T underestimation by KENDA-1 during foehn events are difficult to explain. A~~ 625 2022) and, second, the MWR/MEE has been trained with profiles from Payerne, so that the difference in altitude between both stations (+100 m) and in atmospheric conditions could induce a larger RMSE or even a bias in the MWR measurements. ~~The direct influence of topography (Löhnert et al., 2021) can be discarded, since the instrument has been placed in order to have to obstable in the line of sight. Despite this~~ Despite these uncertainties, the T differences up to -3 °C are probably a clear underestimation of KENDA-1 Ts. The hypothesis of ~~of cloud amount overestimation,~~

cloud
amount overestimation mentioned before can also explain this T profile bias.

4.3.2 ~~Wind~~

~~The valley wind monthly climatology~~ KENDA-1 skill in wind estimate

630 ~~orientation of the Sarneraatal with west facing slopes could allow this persistence but no past study mention this phenomenon. These winds from the pass explains the difference between the along valley wind speeds pattern at MER (Fig. 9) and at MEE~~
The monthly valley wind reveals a ~~very good performance of the model. Up and down-valley wind are well modeled~~
good performance of the model. Up and down-valley wind are in good agreement with the
observations from March to July and, to a lesser extent, in ~~November if compared to the observations. KENDA-1 is also able to get this~~

November. KENDA-1 is also able to get the seasonal evolution of the
vertical extent of the valley wind system. The onset of up valley winds is however predicted ~~with a larger~~
too early after sunrise (Fig. 6 and 8).
This 1-2 hours difference with the observations is partially explained by the absence of surface T inversion in the model (sect. 3.1.3), so the time allowing an erosion of the stable layer is not taken into account.

635 The capability of COSMO models to estimate the diurnal along-valley winds in real valleys has been investigated by Schmidli et al. (2018) for 3 summer weeks with weak synoptic forcing and intense solar heating. The model results are compared to observations at the MeteoSwiss ANETZ stations, the automatic monitoring network preceding the present-day SMN. They showed that the wind diurnal cycle ~~was~~ is well represented by COSMO1-E in large valleys such as the Rhine Valley at Chur (base width of 3 km and width at half height of 8 km), and medium valleys (e.g. the Rhone Valley at Visp a with base width of 1 km

640 ~~valley but with lower wind speeds (10-15 km/h). If the last difference can be also~~ and width at half height of 4 km). For smaller valleys, e.g. the Maggia Valley in Cevio (base width of 500 m, width at half-height
of 3 km), the valley wind amplitude was underestimated. Despite an underestimation of the maximal valley wind speed, the onset of up and down valley winds was correctly modeled. The results of the modeled wind speed and direction at MEE are comparable to the analysis in Visp (Fig. 8), a valley with a similar cross-section. However, the onset of up and down valley winds is in less agreement with the observations at Meiringen, probably due to the four time shorter length of the Haslital and its

645 ~~stronger near the valley outlet (20-30 km/h) that then gradually weaken~~ topographic peculiarities.
The differences between KENDA-1 and the observed cross-valley wind climatology (Fig. 9) can be interpreted as a too

strong ~~influence of the Sarneraatal thermal winds or as an effect of the grid cell overlap on the north-facing slope. The presence~~

~~740 of strong down slope winds at the Brünig pass may have a direct influence on the along valley wind diurnal cycle. In a more~~
modeled influence of the Sarneraatal thermal winds or as an effect of the grid cell overlap on the north-facing slope. The
presence of strong down slope winds at the Brünig Pass may have a direct influence on the along valley wind diurnal cycle.
In a recent study in the Rhone valley at Sion, Schmidli and Quimbayo-Duarte (2023) reports a correctly modeled evening

650 transition but an inadequate representation of the morning wind reversal by ~~COSMO-1E whereas the evening transition is correctly modeled. They showed particularly poor~~
~~performance in along valley wind simulation for certain days in the Rhone valley. The study focuses on results above~~ COSMO-1E. Like in the
Haslital (Fig. ~~13), too strong modeled cross-valley wind reaching~~

9), too strong
modeled cross-valley wind reaching the valley floor interrupt the formation of the up-valley ~~flows.~~ flows for certain days. At Sion, the
cross-valley flow is restricted to upper levels so that the stronger lower valley atmosphere stratification protects the up-valley
flow.

According to (Schmidli et al., 2018), the ~~key factor is not the resolution of the grid. The horizontal resolution required for a good along valley wind representation is moderate. As long as the resolution of the valley base cross section is 1 or 2 grid points width, the results obtained are good in most cases. A more important feature is the altitude bias of the model at the ground. For~~

~~750~~ horizontal resolution required for a good along valley wind representation requests
655 ~~Finally concerning the onset of up valley wind, both the time and the pattern of the transition are similar between~~ at least 1-2 grid cells in the valley base cross section. A more important feature is the altitude bias of the model at the ground.

For the MER station, the width of the valley can contain 1.5 grid cells (Fig. 1) but the fact that no cell ~~is superimposed on the valley floor only~~ contains only the valley
floor leads to this disfavouring ~~altitude bias. Indeed, the two cells overlapping on the valley floor also overlap part of the steep ascending slope. Concerning the problem of stratification that favors the influence of cross-valley winds, surface moisture is a key factor. Simulations performed by Schmidli and Quimbayo-Duarte (2023) show that a 30% increased~~ bias in altitude. Surface atmospheric moisture is a key factor of stratification, which in turn favors
the cross valley winds influence. Simulations performed by Schmidli and Quimbayo-Duarte (2023) show that a 30% increased

soil moisture relative to KENDA-1 data leads to better along valley wind modeling. Even though stronger smoothing of the
~~topography~~

660 ~~lowest atmospheric layer (as Zängl (2004)) and down wind starts at ground~~ topography improves the stratus cloud simulations, it also decrease the quality of forecasts of valley winds and orographically

induced convection (Westerhuis et al., 2021).
Finally, despite the fact that KENDA-1 proposes good ~~climatologies,~~ monthly median values, the case-by-case analysis shows important

differences with ~~measurements, whether they are particular events or not.~~ observations. Non-systematic differences are observed in most profiles. Even ~~35~~

thought these differences show
regular patterns in the case of foehn or valley winds, it is common that unpredictable behavior affects the model.

665 ~~mean~~ 5 Conclusion

The ~~analysis of the data from the MER campaign, in the Haslital,~~ extensive measurement campaign in MER yields valuable information on the ~~climatology of wind profiles and T-profiles. The MWR and DWL installed, as well as the nearby SMN station,~~ diurnal and seasonal cycles of wind and T
profiles that were not available in this region and that are rather sparse in ~~mountainous regions. The main conclusions that can be drawn from the Meiringen campaign are the following:~~

~~—~~alpine middle size valleys. The observations of the
MWR, DWL and of the nearby SMN stations allowed to determine the particularities of ~~this valley between November 2021 and July 2022. This extensive measurement campaign provided data that was not available~~

the Haslital valley between November
2021 and July 2022. In parallel to these observations, the data of two cells of the KENDA-1 assimilation model has been

analyzed. The results in
MER and MEE show similar T profiles. At MEE, the classical valley wind pattern is significantly affected by the tributary valley

670 reversed). A cross-valley phenomena is also measured in MEE from March to August (Fig. 13.a), but especially during analyzed and compared to the measurements.
Regarding the observed and modeled T, the main results concerns the surface based T inversion. Nighttime T inversions are

common commonly observed during all the months under study with bigger amplitudes during December and January. They persist during daytime from November to February.

– The valley wind system is distinguishable in the monthly aggregated values for all the months under study except in
January and a persistence
during daytime from November to February. The frequency of occurrence and the amplitude of the surface T inversions are both underestimated in the T profiles of KENDA-1. This results in a systematic overestimation of the ground T during the presence

675 According to the different monthly climatologies presented, KENDA-1 is generally able to present accurate results regarding the evolution of studied variables even in complex topography. However, some phenomenon specific to mountainous regions and/or particular synoptic conditions can also lead to large modeling errors.

of surface based inversions. In extreme cases it reaches up to 8 °C. This large model error has an important consequence, since
the discrepancies between the model first guess prevents the SMN station
of MER SMN/MER observations to be assimilated. 800 – A T underestimation of -2 to -3 °C under 1500 m, more frequent during nighttime. In July, it is also seen between 2000
and 2500 m during the full daily cycle, except in the early morning.

– KENDA-1 shows a too early onset of up-valley winds due to the absence of the near-surface stable layer caused by the nighttime inversion. The onset of up-valley winds between the ground and 1200 m occurs therefore 1-2 hours earlier than measured.

The differences between
MWR/MEE and KENDA-1/MEE profiles are small with a T underestimation of -2 to -3 °C under 1500 m that is more frequent during nighttime.

Regarding the wind, thermal valley winds are observed in the monthly wind direction for all the months under study except in
680 to measurements of the nearby ground station December and January. This diurnal flow patterns develop in a more distinct way for the summer months (June to August). The

vertical extent of down-valley winds after sunset increases from March to August: from 1000 m.a.g.l. to 1600 m.a.g.l. respectively.

775 – The periods of transition between up and down valley wind are related to sunrise and sunset. The morning transition on the ground is delayed by about 3-4 hours compared to sunrise and is near simultaneous for the rest of the profile.

– The evening transition to down valley winds happens on a shorter time scale both at ground and in the DWL profile.
The onset of down valley winds happens less than an hour before sunset and propagtes from ground to ridge height.

– The influence of m a.g.l. to 1600 m a.g.l. respectively.
The morning transition to up valley wind is delayed by about 3-4 hours compared to sunrise and is near simultaneous for the rest of the profile. The onset of down valley winds happens less than an hour before sunset and propagates from ground to ridge height in some hours. In addition, this thermal wind system can be influenced by external factors such as synoptic

685 show the same diurnal cycle in T difference over a full year. According to the complex topography around MER and the induced elevation bias, the modeled climatology of ground T is satisfactory, wind intrusions or perturbation from from adjacent valleys wind system. Here are the peculiar characteristics observed:

– adjacent valleys wind system. At MEE, N winds from the tributary valley (Sarneraatal)
on the cycle transitions is important below 600 m.a.g.l. even
through the low altitude Brünig Pass are observed from mid-afternoon to sunset. At MEE, they affect the evening transition and sometimes even the along valley wind pattern during daytime below the altitude of the pass. If these N flows only slightly modify the up valley wind direction at MER, they are able to suppress the up valley winds at BRZ. For the climatology of In summer, a cross valley circulation is measured around sunset (19:00-20:00) at MEE with a separation between north and south facing wind between

690 radiation. The observed amplitude difference are mainly due to an underestimation of T at ground (Fig. 6 and 5). 700 and 1000 m a.g.l. The formation of this closed circulation cell is influenced by the strong wind from the Sarneraatal.

The comparison with observations shows that KENDA-1 was able to simulate ~~climatologies in close agreement with~~ median directions and speeds of the diurnal
valley winds. The vertical extent of the thermal winds, the onset time of down valley winds and the interaction with synoptic
winds are also appropriately modeled. However, ~~some phenomena are not~~

KENDA-1 shows a too early (1-2 hours) onset of up-valley winds due to the
absence of the near surface stable layer caused by the nighttime inversion. Moreover, the observed cross circulation in MEE at

695 sunset is not modeled by KENDA-1.
Contrarily to monthly values, the analysis of single profiles shows important differences between the model and the

measurements. This is particularly true during foehn events with a ~~systematic cold bias, a delayed time of foehn breakthrough and the associated overestimated wind speeds.~~

~~- In the case of~~ near systematic underestimation of 2 to 4°C by KENDA-1
in both the ground and the profile temperatures. ~~SMN ground measurements are also used for the description of T inversions.~~

~~The evolution of T in MEE from February to July~~ Wind speeds simulation during foehn show significant difference over MEE
and MER: the ~~KENDA-1 MEE profile show a good match up to 1000 m.a.g.l. whereas the winds over MER are reported to be twice as high~~ KENDA-1/MEE show a good match up to 1000 m a.g.l. whereas KENDA-1/ MER reports wind speed twice

700 higher (120 km/h). A detailed analysis of three clear sky summer days also allows to underline clear differences between the observations and the model concerning the wind direction (up to 90°), the wind speed (up to 30 km/h) and the timing (up to 4-6 h) of the along valley transition.

The results obtained in this study allowed to deepen consensual knowledge about atmospheric phenomena in complex
topography and to identify processes specific to the studied valley. Complex interactions between the Haslital and the tributary

705 valley of the Sarneraatal have been observed and could explain some differences observed with the literature. However, many
observed phenomena are not yet satisfactorily ~~observed~~ characterized and modeled and require further investigation. A better understanding
of the exchange processes in complex topography and the ability of the model to take them into account is an essential condition
to improve the prediction capacity of NWP in ~~complex topography.~~

mountainous terrain.

Data availability. Data are available on request

710 ~~showed that random error~~ Author contributions. AB did the analysis, AB and MCC prepared the manuscript. MH and SM operated the instruments during the campaign.
DL and MA provided the model data. All co-authors contributed to the manuscript online.

Competing interests. The authors declare that they have no conflict of interest.

Acknowledgement. This work was supported by the the Swiss Federal Office for Meteorology and Climatology

~~warm weather, mean maximum up valley velocities of 30-35 km/h are found above the Rhone valley between 15:00 and 16:00 at altitudes around 200 m.a.g.l. Similar timing for maximum up valley winds are found at both MER and MEE, but with reduced speed both at ground in MER (20-30~~ References

715 ~~et al., 2022). KENDA-1 T remains mainly inside the uncertainty. Moreover, the Meiringen radiometer has been trained with profiles from Payerne on the Swiss Plateau, so that the difference in altitude~~ Adler, B., Gohm, A., Kalthoff, N., Babić, N., Corsmeier, U., Lehner, M., Rotach, M. W., Haid, M., Markmann, P., Gast, E., Tsaknakis, G., and
Georgoussis, G.: CROSSINN: A Field Experiment to Study the Three-Dimensional Flow Structure in the Inn Valley, Austria, Bull. Amer. Meteor. Soc., 102, E38 – E60, https://doi.org/10.1175/BAMS-D-19-0283.1, 2021.

Baldauf, M., Seifert, A., Förstner, J., Majewski, D., Raschendorfer, M., and Reinhardt, T.: Operational Convective-Scale Numerical Weather Prediction with the COSMO Model: Description and Sensitivities, Monthly Weather Review, 139, 3887 – 3905,

720 mentioned for the problem of T inversions, https://doi.org/https://doi.org/10.1175/MWR-D-10-05013.1, 2011.
Chachere, C. N. and Pu, Z.: Connections Between Cold Air Pools and Mountain Valley Fog Events in Salt Lake City, Pure Appl. Geophys.,

173, 3187–3196, https://doi.org/10.1007/s00024-016-1316-x, 2017.
Chow, F. K., Weigel, A. P., Street, R. L., Rotach, M. W., and Xue, M.: High-Resolution Large-Eddy Simulations of Flow in a Steep Alpine Valley.

Part I: Methodology, Verification, and Sensitivity Experiments, J. Appl. Meteor. Climatol., 45, 63 – 86, https://doi.org/10.1175/JAM2322.1,
725 inaccuracy. KENDA-1 places the transition to up-valley wind too early after sunrise (Fig. 8 and 11). This 1-2 hours difference

with the observations is partially explained by the absence of surface T inversion in the model (section ??), so the time allowing an erosion of the stable layer is not taken into account.

2006.

Colette, A., Chow, F. K., and Street, R. L.: A Numerical Study of Inversion-Layer Breakup and the Effects of Topographic Shading in Idealized Valleys, J. Appl. Meteor., 42, 1255 – 1272, https://doi.org/https://doi.org/10.1175/1520-0450(2003)042<1255:ANSOIB>2.0.CO;2, 2003.

Crezee, B., Merker, C., Daniel, R., Leuenberger, D., Vural, J., Haefele, A., Hervo, M., Martucci, G., Bättig, P., and Arpagaus, M.: Assimilation of ground-based remote sensing profiler data at MeteoSwiss, EMS Annual Meeting Abstracts, 19, https://doi.org/10.5194/ems2022-568,

730 measurements 2022.
De Wekker, S. F. J. and Kossmann, M.: Convective Boundary Layer Heights Over Mountainous Terrain—A Review of Concepts, Frontiers in

Earth Science, 3, https://doi.org/10.3389/feart.2015.00077, 2015.
Diémoz, H., Barnaba, F., Magri, T., Pession, G., Dionisi, D., Pittavino, S., Tombolato, I. K. F., Campanelli, M., Della Ceca, L. S., Hervo, M.,

Di Liberto, L., Ferrero, L., and Gobbi, G. P.: Transport of Po Valley aerosol pollution to the northwestern Alps – Part 1: Phenomenology,
735 speed, the onset of up and down valley winds was correctly modeled. The results of the modeled wind speed and direction at MEE are comparable to the analysis in Visp (Fig. 11). However, the onset of up and down valley winds is less well modeled in the Haslital. The valleys at both sites have a similar cross-sections but the Rhone valley is four time longer than the Haslital.

The differences between KENDA-1 and the observed cross-valley wind climatology (Fig. 13) Atmos. Chem. Phys., 19, 3065–3095, https://doi.org/10.5194/acp-19-3065-2019, 2019.

Duine, G.-J., Hedde, T., Roubin, P., Durand, P., Lothon, M., Lohou, F., Augustin, P., and Fourmentin, M.: Characterization of valley flows
845 within two confluent valleys under stable conditions: observations from the KASCADE field experiment, Quart. J. Roy. Meteor. Soc., 143, 1886–1902, https://doi.org/10.1002/qj.3049, 2017.

Dürr, B.: Automatisiertes Verfahren zur Bestimmung von Föhn in Alpentälern, Tech. rep., Arbeitsberichte der MeteoSchweiz, 223, 22

pp, https://www.meteoschweiz.admin.ch/dam/jcr:3ed2aec8-0901-417a-acc3-8be11cce440a/Foehnindex_Arbeitsbericht_223_Automatisiertes_Verfahren_zur_Bestimmung_von_Foehn_in_Alpentaelern_de.pdf, 2008.

https:
740 //www.meteoschweiz.admin.ch/dam/jcr:3ed2aec8-0901-417a-acc3-8be11cce440a/Foehnindex_Arbeitsbericht_223_Automatisiertes_

Verfahren_zur_Bestimmung_von_Foehn_in_Alpentaelern_de.pdf, 2008.
Giovannini, L., Laiti, L., Serafin, S., and Zardi, D.: The thermally driven diurnal wind system of the Adige Valley in the Italian Alps, Quart. J.

Roy. Meteor. Soc., 143, 2389–2402, https://doi.org/10.1002/qj.3092, 2017.
Hauge, G.: High resolution weather forecasting and predictability - applications in complex terrain, Ph.D. thesis, University of Bergen, https://core.ac.uk/
download/pdf/30925119.pdf, Sweden,

745 https://core.ac.uk/download/pdf/30925119.pdf, 2006.
Hervo, M., Bättig, P., and Haefele, A.: Evaluation of the new microwave radiometer HATPRO-G5., MeteoSwiss, Payerne, Switzerland, 2021.
855 Tech. rep., Federal Office of Meteorology

and Climatology, MeteoSwiss, Payerne, Switzerland, 2021.
Hiebl, J. and Schöner, W.: Temperature inversions in Austria in a warming climate changes in space and time, Meteorologische Zeitschrift, 27,

https://doi.org/10.1127/metz/2018/0899, 2018.

between 0 to 1500 m.a.g.l (Fig. 8.a) from June apart. Indeed, the same is observed by Schmid et al. (2020) at the same season and by Giovannini et al. (2017) for which almost all cases are in spring and summer. The fact that

750 Hunt, B. R., Kostelich, E. J., and Szunyogh, I.: Efficient data assimilation for spatiotemporal chaos: A local ensemble transform Kalman filter, Physica D: Nonlinear Phenomena, 230, 112–126, https://doi.org/10.1016/j.physd.2006.11.008, 2007.

39

Jacques-Coper, M., Falvey, M., and Muñoz, R. C.: Inter-daily variability of a strong thermally-driven wind system over the Atacama Desert
860 of South America: synoptic forcing and short-term predictability using the GFS global model, Theor. and Appl. Clim., 121, 211–223, https://doi.org/10.1007/s00704-014-1231-y, 2015.

755 Jansing, L., Papritz, L., Dürr, B., Gerstgrasser, D., and Sprenger, M.: Classification of Alpine south foehn based on 5 years of kilometre-scale analysis data, Weather and Climate Dyn., 3, 1113–1138, https://doi.org/10.5194/wcd-3-1113-2022, 2022.

Joly, D. and Richard, Y.: Topographic descriptors and thermal inversions amid the plateaus and mountains of the Jura (France), Climatologie,
865 15, 46–61, https://doi.org/10.4267/climatologie.1335, 2018.

Joly, D. and Richard, Y.: Frequency, intensity, and duration of thermal inversions in the Jura Mountains of France, Theor. Appl. Climatol., 138,
760 affects the model (Fig. J1, H1).

639–655, https://doi.org/10.1007/s00704-019-02855-3, 2019.

Kossmann, M. and Sturman, A.: Pressure-Driven Channeling Effects in Bent Valleys, J. Appl. Meteorol., 42, 151–158, https://doi.org/10.1175/1520-0450(2003)042<0151:PDCEIB>2.0.CO;2, 2003.

870 Krishnamurthy, R., Calhoun, R., Billings, B., and Doyle, J.: Wind turbulence estimates in a valley by coherent Doppler lidar, Meteor. Appl., 18, 361–371, https://doi.org/10.1002/met.263, 2011.

765 Lang, M. N., Gohm, A., and Wagner, J. S.: The impact of embedded valleys on daytime pollution transport over a mountain range, Atmos. Chem. Phys., 15, 11 981–11 998, https://doi.org/10.5194/acp-15-11981-2015, 2015.

Langhans, W., Schmidli, J., Fuhrer, O., Bieri, S., and Schär, C.: Long-Term Simulations of Thermally Driven Flows and Orographic Convection
875 at Convection-Parameterizing and Cloud-Resolving Resolutions, J. Appl. Meteor. Climatol., 52, 1490 – 1510, https://doi.org/10.1175/JAMC-D-12-0167.1, 2013.

770 December and January. In addition, this thermal wind system can be influenced by external factors such as synoptic Lehner, M. and Rotach, M. W.: Current Challenges in Understanding and Predicting Transport and Exchange in the Atmosphere over Mountainous Terrain, Atmosphere, 9, https://doi.org/10.3390/atmos9070276, 2018.

Leuenberger, D., Koller, M., Fuhrer, O., and Schär, C.: A Generalization of the SLEVE Vertical Coordinate, Mon. Wea. Rev., 138, 3683 – 3689, https://doi.org/10.1175/2010MWR3307.1, 2010.

Liu, M., Liu, Y.-A., and Shu, J.: Characteristics Analysis of the Multi-Channel Ground-Based Microwave Radiometer Observations during
880 775 Various Weather Conditions, Atmosphere, 13, https://doi.org/10.3390/atmos13101556, 2022.

Lute, A. C. and Abatzoglou, J. T.: Best practices for estimating near-surface air temperature lapse rates, Int. J. Climatol., 41, E110–E125, https://doi.org/10.1002/joc.6668, 2021.

Löhnert, U. and Maier, O.: Atmospheric Operational profiling of temperature using ground-based microwave radiometry at Payerne: prospects and challenges, Atmos. Meas. Tech., 5, 1121–1134, https://doi.org/10.5194/amt-5-1121-2012, 2012.

885 780 during calm clear days. These strong winds can easily exceed the Haslital along up valley winds.

– A cross valley circulation is measured around sunset (19:00-20:00). A separation between north and south facing wind lays between 700 and 1000 m.a.g.l. which suggests that flow pattern form a closed circulation cell. This mechanism is influenced by the strong wind from the Sarneraatal.

– Foehn is able to rapidly (<1 hr) destroy the T inversion if present. The delay between the T increase due to the
Löhnert, U., Knist, C., Böck, T., and Pospichal, B.: Brightness Temperatures from boundary layer scans, Microwave Radiometer Observations. University of Cologne DWD Lindenberg [data set], Microwave Radiometer Observations during FESSTVaL 2021, when three radio soundings (RS) were performed
https://doi.org/10.25592/uhhfdm.10198, 2021.

Project: FESSTVaL (Field Experiment on submesoscale spatio-temporal variability in Lindenberg), a measurement campaign initiated by the Hans-Ertel-Center for Weather Research., 2022.

Martinet, P., Cimini, D., De Angelis, F., Canut, G., Unger, V., Guillot, R., Tzanos, D., and Paci, A.: Combining ground-based microwave

radiometer and the AROME convective scale model through 1DVAR retrievals in complex terrain: an Alpine valley case study, Atmos.Meas.

785 ~~foehn breakthrough can be of 1-2 hr between the SMN/MER ground measurement and the MWR/MEE lowest level.~~

~~Maximum wind speeds are homogeneous between ground and 1500 m.a.g.l. which corresponds to mean ridge's height (valley channeling).~~

~~36~~

Tech., 10, 3385–3402, https://doi.org/10.5194/amt-10-3385-2017, 2017.
~~890~~ Miró, J. R., Peña, J. C., Pepin, N., Sairouni, A., and Aran, M.: Key features of cold-air pool episodes in the northeast of the Iberian Peninsula

(Cerdanya, eastern Pyrenees), Int. J. of Climatol., 38, 1105–1115, https://doi.org/https://doi.org/10.1002/joc.5236, 2018.

~~Nipen, T., Seierstad, I., Lussana, C., Kristiansen, J., and Hov, : Adopting Citizen Observations in Operational Weather Prediction, Bull. Amer. Meteor. Soc., 101, E43 – E57, https://doi.org/10.1175/BAMS-D-18-0237.1, 2020.~~

33

Rose, T., Crewell, S., Löhnert, U., and Simmer, C.: A network suitable microwave radiometer for operational monitoring of the cloudy
~~895~~ atmosphere, Atmos. Res., 75, 183–200, https://doi.org/10.1016/j.atmosres.2004.12.005, 2005.

~~40~~

790 ~~of the Sarneraatal. Additionally, during foehn events, wind speeds at MER are almost two times higher than at MEE. The comparison with observations show~~ Rotach, M. W., Gohm, A., Lang, M. N., Leukauf, D., Stiperski, I., and Wagner, J. S.: On the Vertical Exchange of Heat, Mass, and Momentum
Over Complex, Mountainous Terrain, Frontiers in Earth Science, 3, https://doi.org/10.3389/feart.2015.00076, 2015.

Rotach, M. W., Serafin, S., Ward, H. C., Arpagaus, M., Colfescu, I., Cuxart, J., De Wekker, S. F. J., Grubišic, V., Kalthoff, N., Karl, T., Kirshbaum, D. J., Lehner, M., Mobbs, S., Paci, A., Palazzi, E., Bailey, A., Schmidli, J., Wittmann, C., Wohlfahrt, G., and Zardi, D.: A Collaborative Effort to Better Understand, Measure, and Model Atmospheric Exchange Processes over Mountains, Bulletin of the American

795 ~~properly captured by the model in assimilation mode:~~

~~– The frequency of occurrence and the amplitude of the surface T inversion are both underestimated in the T profiles of KENDA-1. This results in a systematic overestimation of the ground T during the presence of surface based inversions. In extreme cases it reaches up to 9 °C. Moreover,~~ Meteorological Society, 103, E1282 – E1295, https://doi.org/https://doi.org/10.1175/BAMS-D-21-0232.1, 2022.
Rupp, D. E., Shafer, S. L., Daly, C., Jones, J. A., and Frey, S. J. K.: Temperature Gradients and Inversions in a Forested Cascade Range Basin:

Synoptic- to Local-Scale Controls, J. Geophys. Res. Atmos., 125, e2020JD032 686, https://doi.org/10.1029/2020JD032686, 2020.
Saigger, M. and Gohm, A.: Is it north or west foehn? A Lagrangian analysis of Penetration and Interruption of Alpine Foehn intensive

observation period 1 (PIANO IOP 1), Weather and Climate Dyn., 3, 279–303, https://doi.org/10.5194/wcd-3-279-2022, 2022.
~~900~~ 800 Schmid, F., Schmidli, J., Hervo, M., and Haefele, A.: Diurnal Valley Winds in a Deep Alpine Valley: Observations, Atmosphere, 11,

https://doi.org/10.3390/atmos11010054, 2020.
Schmidli, J. and Quimbayo-Duarte, J.: Diurnal Valley Winds in a Deep Alpine Valley: Model Results, Meteorology, 2, 87–106,

https://doi.org/10.3390/meteorology2010007, 2023.
Schmidli, J. and Rotunno, R.: Mechanisms of Along-Valley Winds and Heat Exchange over Mountainous Terrain, J. Atmos. Sci., 67, 3033 –

~~905~~ 805 ~~– Contrarily to climatologies, the analysis of single profiles show important differences with~~ 3047, https://doi.org/10.1175/2010JAS3473.1, 2010.
Schmidli, J., Böing, S., and Fuhrer, O.: Accuracy of Simulated Diurnal Valley Winds in the Swiss Alps: Influence of Grid Resolution,

Topography Filtering, and Land Surface Datasets, Atmosphere, 9, https://doi.org/10.3390/atmos9050196, 2018.
Schnitzhofer, R., Norman, M., Wisthaler, A., Vergeiner, J., Harnisch, F., Gohm, A., Obleitner, F., Fix, A., Neininger, B., and Hansel, A.: A

multimethodological approach to study the spatial distribution of air pollution in an Alpine valley during wintertime, Atmos. Chem. ~~and~~

~~910 Phys.,~~ Phys.,
810 ~~foehn breakthrough until maximal wind speed is reached, the difference then gradually decreases.~~

–9, 3385–3396, https://doi.org/10.5194/acp-9-3385-2009, 2009.

Schraff, C., Reich, H., Rhodin, A., Schomburg, A., Stephan, K., Periáñez, A., and Potthast, R.: Kilometre-scale ensemble data assimilation for the COSMO model (KENDA), Quart. J. Roy. Meteor. Soc., 142, 1453–1472, https://doi.org/10.1002/qj.2748, 2016.

Sekula, P., Bokwa, A., Bochenek, B., and Zimnoch, M.: Prediction of Air Temperature in the Polish Western Carpathian Mountains with the ALADIN-HIRLAM Numerical Weather Prediction System, Atmosphere, 10, https://doi.org/10.3390/atmos10040186, 2019.

915 815 Serafin, S., Adler, B., Cuxart, J., De Wekker, S. F. J., Gohm, A., Grisogono, B., Kalthoff, N., Kirshbaum, D. J., Rotach, M. W., Schmidli, J., Stiperski, I., Večenaj, , and Zardi, D.: Exchange Processes in the Atmospheric Boundary Layer Over Mountainous Terrain, Atmosphere, 9, https://doi.org/10.3390/atmos9030102, 2018.

Sfyri, E., Rotach, M. W., Stiperski, I., Bosveld, F. C., Lehner, M., and Obleitner, F.: Scalar-Flux Similarity in the Layer Near the Surface Over Mountainous Terrain, Boundary-Layer Meteorology, 169, 11–46, https://doi.org/10.1007/s10546-018-0365-3, 2018.

920 820 Stephan, K., Klink, S., and Schraff, C.: Assimilation of radar-derived rain rates into the convective-scale model COSMO-DE at DWD, Quart. J. Roy. Meteor. Soc., 134, 1315–1326, https://doi.org/10.1002/qj.269, 2008.

Tian, Y., Schmidli, J., and Quimbayo-Duarte, J.: A station-based evaluation of south foehn forecasting with COSMO-1, EGU General Assembly, Vienna, Austria, https://doi.org/10.5194/egusphere-egu22-3680, 2022.

Vosper, S., Carter, E., Lean, H., Lock, A., Clark, P., and Webster, S.: High resolution modelling of valley cold pools, Atmos. Sci. Letters, 14, 925 825 193–199, https://doi.org/https://doi.org/10.1002/asl2.439, 2013.

Voudouri, A., Khain, P., Carmona, I., Avgoustoglou, E., Kaufmann, P., Grazzini, F., and Bettems, J.: Optimization of high resolution COSMO model performance over Switzerland and Northern Italy, Atmos. Res., 213, 70–85, https://doi.org/10.1016/j.atmosres.2018.05.026, 2018.

seasonal evolution of the vertical extent of the valley wind system. The onset of Voudouri, A., Avgoustoglou, E., Carmona, I., Levi, Y., Bucchignani, E., Kaufmann, P., and Bettems, J.-M.: Objective Calibration
of Numerical Weather Prediction Model: Application on Fine Resolution COSMO Model over Switzerland, Atmosphere, 12, 930 https://doi.org/10.3390/atmos12101358, 2021.

Wagner, J. S., Gohm, A., and Rotach, M. W.: The Impact of Horizontal Model Grid Resolution on the Boundary Layer Structure over an 830 Idealized Valley, Mon. Wea. Rev., 142, 3446 – 3465, https://doi.org/10.1175/MWR-D-14-00002.1, 2014.

Wang, Y., Hocut, C. M., Hoch, S. W., Creegan, E., Fernando, H. J. S., Whiteman, C. D., Felton, M., and Huynh, G.: Triple Doppler
wind lidar observations during the mountain terrain atmospheric modeling and observations field campaign., Journal of Applied Remote Sensing, 10,

935 J. Appl. Rem. Sens., 10,
https://doi.org/10.1117/1.JRS.10.026015, 2016.

Westerhuis, S., Fuhrer, O., Bhattacharya, R., Schmidli, J., and Bretherton, C.: Effects of terrain-following vertical coordinates on simulation of 835 stratus clouds in numerical weather prediction models, Quart. J. Roy. Meteor. Soc., 147, 94–105, https://doi.org/10.1002/qj.3907, 2021.

Whiteman, C. D.: Observations of Thermally Developed Wind Systems in Mountainous Terrain, Environmental Science, pp. 5–42, https://doi.org/10.1007/978-1-935704-25-6_2, 1990.

940 Zardi, D. and Whiteman, C. D.: Observations of thermally developed wind systems in mountainous terrain. Mountain Weather Research and Forecasting—Recent Progress and Current Challenges, Springer: Berlin, Germany, pp. 35–122, 2013.

840 2022.
Zängl, G.: A reexamination of the valley wind system in the Alpine Inn Valley with numerical simulations, Meteor. Atmos. Phys., 87, 241–256, https://doi.org/10.1007/s00703-003-0056-5, 2004.

Appendix A: Weather conditions

Temp. [°C] Precip. [mm] % max sunshine
Abs. % Norm Abs. % Norm Abs. % Norm

Nov 3.1 [HTML]ECF4FF-0.6 57.8 [HTML]FFCE9361.03 38 [HTML]FFFFFF90
Dec -1.5 [HTML]DAE8FC-1 119 [HTML]DAE8FC121.93 30 [HTML]FFFFFF90
Jan -2 [HTML]DAE8FC-0.9 35 [HTML]FFCE9342.42 54 [HTML]FFCE93130
Feb 2.2 [HTML]FFCE93+1.8 90.5 [HTML]DAE8FC125.52 54 [HTML]FFCE93120
Mar 6.4 [HTML]FFCE93+1.4 17.6 [HTML]FFCCC920.71 70 [HTML]FFCCC9150
Apr 8.8 [HTML]ECF4FF-0.4 74.4 [HTML]FFFFC782.85 54 [HTML]FFFFFF110
May 15.3 [HTML]FFCCC9+2.1 47.2 [HTML]FFCCC934.43 48 [HTML]FFFFFF110
Jun 18.7 [HTML]FFCCC9+2.2 142 [HTML]FFFFFF95.95 53 [HTML]FFFFFF110
Jul 20.4 [HTML]FFCCC9+2.5 72.5 [HTML]FFCE9345.26 62 [HTML]FFCE93130
Aug 19.7 [HTML]FFCCC9+2.3 89.7 [HTML]FFCE9351.49 61 [HTML]FFCE93120

Table A1. Absolute values and ratios to the climatological norm (1991-2020) for monthly temperature, total precipitation and proportion of max. sunshine duration in the SMN station from MER.

Figure A1. Timeseries of precipitation intensity [mm/10mm] (blue bar), cumulative precipitation [mm] (blue line) and mean sunshine duration [min/10min] over (5 days moving average)

945 Appendix B: Geographical description

Figure B1. Map of the geographical situation in the lower Haslital (E-W and the Sarneraatal (S-N). The automatic measurement from the SMN are: Meiringen (MER), Brienz (BRZ) and Giswil (GIH). Stations from the FEDRO are also depicted: Brünig (BRU), Lungern (LUN) and Buchholzbrücke (BUC). The last represented site is the campaign site in Unterbach (MEE). ©swisstopo

Figure B2. Along-valley altitude variation for the two crests (red/blue) and valley floor (shadowed). Valley floor width is depicted with the dotted pink line. The abscissa indicates the distance from the top of the valley (Grimselpass) following the valley lowest point.

Appendix C: MWR vertical resolution

Range [m.a.g.l.] Vertical resolution [m] RMSE [°C]
0-250 50 0.25
250-500 75 0.25
500-800 100 0.50
800-1200 150 0.50
1200-1600 150 0.75
1600-2200 200 1.00
2200-3000 300 1.00

Table C1. Vertical resolution and RMS error (given by the manufacturer) of the MWR temperature according to its different ranges.

Figure D1. MWR temporal T gradient climatology [°C/hr]. Sunset and sunrise are depicted with the dotted lines.

Appendix D: T gradient climatology

00:00
3000 03:00 06:00 09:00 15:00 18:00

3000 3000 3000 3000 3000

KENDA-1

MWR

SMN MER
2500

2500 2500 2500 2500 2500

2000
2000 2000 2000 2000 2000

1500
1500 1500 1500 1500 1500

1000
1000 1000 1000 1000 1000

500 500 500 500 500 500
0 5 10 15

800 0 5 10 15 0 5 10 15 0 5 10 15 0 5 10 15 0 5 10 15
800 800 800 800 800

750 750 750 750 750 750

700 700 700 700 700 700

650 650 650 650 650 650

600 600 600 600 600 600

0 5 10 15 0 5 10 15 0 5 10 15 0 5 10 15 0 5 10 15 0 5 10 15

T [°C] T [°C] T [°C] T [°C] T [°C] T [°C]

Figure E1. T-profile from MWR (blue) and KENDA-1 (red) for the 22.03.2022. The dashed line indicates the raw value of KENDA-1 as it is used in the ground T comparison. The dash-dotted line extends the profile to the ground with the same gradient as the MWR measurement.

00:00 03:00 06:00
3000 3000 3000

KENDA-1

MWR

2500 SMN MER 2500 2500

2000 2000 2000

1500 1500 1500

1000 1000 1000

500 500 500
10 15 20 25 30 10 15 20 25 30 10 15 20 25 30

800 800 800

750 750 750

700 700 700

650 650 650

600 600 600

10 15 20 25 30 10 15 20 25 30 10 15 20 25 30

T [°C] T [°C] T [°C]

Figure E2. T-profile from MWR (blue) and KENDA-1 (red) for the 19.07.2022. The dashed line indicates the raw value of KENDA-1 as it is used in the ground T comparison. The dash-dotted line extends the profile to the ground with the same gradient as the MWR measurement..

Appendix E: T-inversion at the end of March

47

a) T
T-profiles RS/KENDA-1 MER 17.11.2021 b) KENDA-RS

3000 T 3000
RS

T
KENDA-1

2500 2500

2000 2000

1500 1500

1000 1000

08:30 UTC
500 500

-4 -2 0 2 4
-4 -3 -2 -1 0 1 2 3 4 5 6

3000 3000

2500 2500

2000 2000

1500 1500

1000 1000

11:00 UTC c) T-profile RS PAY 17.11.2021

500 500
-4 -2 0 2 4

-4 -3 -2 -1 0 1 2 3 4 5 6
3000

3000 3000

2500

2500 2500

2000

2000 2000

1500
1500 1500

1000 1000
1000

14:00 UTC 12.00 UTC
500 500 500

-4 -2 0 2 4
-4 -2 0 2 4 6 T [°C] -4 -3 -2 -1 0 1 2 3 4 5 6

~~T [°C] T [°C]~~

~~Figure F1. a) T-profiles of RS (in green) and KENDA-1 (in red) at MER during the day of 17.11.2022 at 08:30, 11:00 and 14:00. For the top plot, the T-profile of KENDA-1 at 08:00, 09:00 and their average are plotted~~ 35

> Very nice and simple application that allows me to quickly and easily display the differences between two similar files.

> It can't be much easier to compare two files. Comparing two revisions of a document becomes quite easy thanks to this tool.

Questions and Answers

How can I compare two PDF files?

Is it secure to use PDF24 Tools?

Can I use PDF24 on a Mac, Linux or Smartphone?

Can I use PDF24 offline without an Internet connection?

+ Ask a new question +

Please rate this app

☆ ☆ ☆ ☆ ☆

Your impressions and thoughts. Please rate fairly.

Submit

Please report problems here →

Please share this page

Help our new, cool and free tools to grow!

Write an article about our tools on your forum, blog or website.

Alternative: PDF24 Creator

Software for Windows with similar features

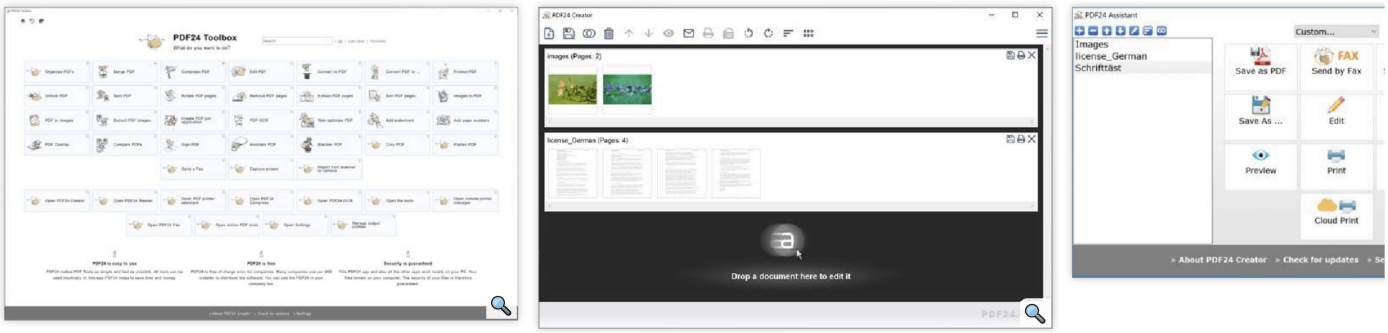

PDF24 Creator →

More great tools

All | Last used | Favorites | Search

Merge PDF | Split PDF | Compress PDF | Edit PDF | Sign PDF

PDF Converter | Images to PDF | PDF to images | Extract PDF images | Protect PDF

Unlock PDF | Rotate PDF pages | Remove PDF pages | Extract PDF pages | Rearrange PDF pages

Webpage to PDF | Create PDF job application | Create PDF with a camera | PDF OCR | Add watermark

Add page numbers | View as PDF | PDF Overlay | Compare PDFs | Web optimize PDF

Annotate PDF | Redact PDF | Create PDF | PDF to Word | JPG to PDF

All tools